STUDIES OF THE CYTOCHROME bc_1 COMPLEX FROM *RHODOBACTER SPHAEROIDES*

By

MARIA ELBERRY

Masters of Science
Oklahoma State University
Oklahoma, United States
2005

Bachelor of Science
Lebanese American University
Byblos, Lebanon
2002

Submitted to the Faculty of the
Graduate College of the
Oklahoma State University
in partial fulfillment of
the requirements for the degree of
DOCTOR OF PHILOSOPHY
Jul 2008

STUDIES OF THE CYTOCHROME bc_1 COMPLEX FROM

RHODOBACTER SPHAEROIDES

Thesis Approved:

Dr. Chang-An Yu

Dr. Linda Yu

Dr. Robert Burnap

Dr. Robert Matts

Dr. Gordon Emslie

ACKNOWLEDGEMENTS

I deeply thank my parents, Antoine and Joumana Elberry, for their encouragement, moral and financial support.

I wish to express my sincere gratitude to my advisor Dr. Chang-An Yu for his supervision, inspiration and encouragement throughout my graduate program. I am also equally grateful to Dr. Linda Yu for her motivation and support during my study. My sincere appreciation extends to my graduate committee members Dr. Robert Matts and Dr. Robert Burnap for their assistance and guidance. I would also like to thank Dr. Di Xia for his collaboration and support and above all for his valuable advices.

I also thank all professors and staff of the Biochemistry and Molecular Biology department and all the former and current students of Dr Yu's lab, especially Dr. Shih-Chia Tso (Scott), Dr. Kunhung Xiao (Kevin) and Dr. Hewen Ma (Katherine).

TABLE OF CONTENTS

Chapter Page

LIST OF FIGURES

LIST OF FIGURES

Figure Page

LIST OF TABLES

NOMENCLATURE

ADP	Adenosine di-phosphate
ATP	Adenosine tri-phosphate
Asc	Ascorbate
bc_1	Ubiquinol-cytochrome *c* oxidoreductase
b_H	Higher potential cytochrome *b* heme
b_L	Lower potential cytochrome *b* heme
Cyt	Cytochrome
CO	Carbon monoxide
DNA	Deoxyribonucleic Acid
DSC	Differential scanning calorimetry
E. coli	*Escherichia coli*
EDTA	Ethylenediaminetetramethylacetic acid
Em	Midpoint potential
FAD	Flavin adenosine dinucleotide – oxidized form
$FADH_2$	Flavin adenosine dinucleotide – reduced form
HD	Head domain
HRP	horseradish peroxidase
ICM	Intracytoplasmic membrane
ISP	Iron-Sulfur Protein

KDa	Kilo Daltons
Kb	Kilo Base-pairs
LB	Luria Broth
ME	Mercaptoethanol
NAD	Nicotinamide adenosine dinucleotide – oxidized form
$NADH_2$	Nicotinamide adenosine dinucleotide – reduced form
PAGE	Polyacrylamide gel electrophoresis
Pi	Inroganic phosphate
Q	Ubiquinone
$QH^{\cdot}$	Semiubiquinone
QH_2	Ubiquinol
Qi	Inside ubiquinol site
Qo	Outside ubiquinone site
$Q_0C_{10}BrH_2$	2,3-Dimethoxy-5-methyl-6-(10-bromodecyl)-1,4-benzoquinol
Rb.	*Rhodobacter*
SDS	Sodium dodecyl sulfate
SR	Super Reductase mutant
Tm	Melting temperature
TMBZ	3,3',5,5'-tetramethyl benzidine dihydrochloride
UV	Ultra Violet
[2Fe2S]	Iron-sulfur cluster

CHAPTER I

INTRODUCTION

A. Mitochondrial respiratory chain

The eukaryotic mitochondrion is responsible of several essential functions in the cell. Its major function is to generate energy for cellular activity through oxidative phosphorylation (Fig. 1), which is based on the sequential operation of five protein complexes, complexes I through V, four of which constitute the mitochondrial electron transfer chain; complexes I through IV. NADH and succinate, two products of the citric acid cycle, are electron donors of the electron transfer chain through complex I and complex II, respectively. Complex I, NADH-ubiquinone oxidoreductase, transfers electrons from NADH to ubiquinone. Complex II, succinate-ubiquinone oxidoreductase, transfers electrons from succinate to ubiquinone. Ubiquinol reduces complex III, ubiquinol-cytochrome *c* reductase, which transfers the electron through cytochrome *c* to complex IV, cytochrome *c* oxidase. The final electron acceptor in the electron transfer chain is oxygen. For the exception of complex II, electron transfer through these complexes is coupled to proton translocation from the matrix into the inter-membrane space, establishing a proton gradient across the inner membrane. Complex V, ATP synthase, uses this transmembrane proton gradient to drive the endergonic reaction of

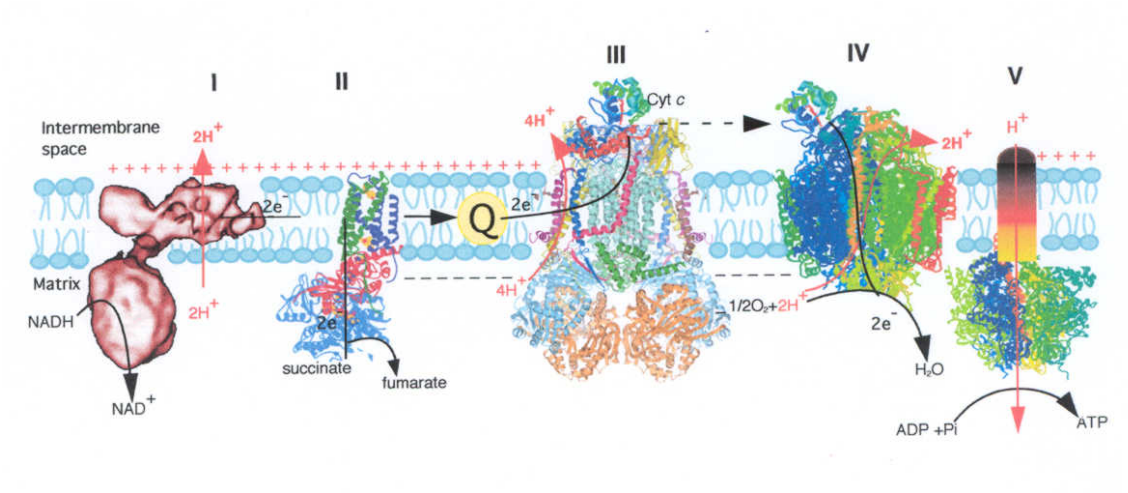

Figure 1: Mitochondrial electron transport chain complexes. Black arrows and dashed arrows illustrate proton translocation and electron transport, respectively.

ATP synthesis. Complex V exchanges the gradient's osmotic energy into chemical energy, a conversion known as the chemiosmotic coupling process.

In the aerobic respiratory system of bacteria, complex III, also referred to as the cytochrome bc_1 complex, perform a similar function as in the mitochondria. In chloroplasts and cyanobacteria, the bc_1 complex is substituted by a similar complex called the cytochrome b_6f or plastoquinol-plastocyanin oxidoreductase that performs the same function in the electron transfer chain. Similarity between the two complexes is high enough to believe most features discussed about one complex apply to the other.

B. The cytochrome bc_1 complex

The cytochrome bc_1 complex is a vital constituent of the electron transfer pathway of mitochondria and many respiratory and photosynthetic bacteria (1-5). It catalyzes the electron transfer from quinol to a *c*-type cytochrome with generation of a proton gradient used for ATP synthesis. All cytochrome bc_1 complexes contain three redox subunits (Table 1) housing four redox centers: cytochrome *b*, which houses two *b*-type hemes (b_L or b_{566} and b_H or b_{562}), cytochrome c_1 which houses a *c*-type heme and the Rieske iron-sulfur protein, which houses a high-potential [2Fe2S] cluster (4). Some cytochrome bc_1 complexes consist of additional supernumerary subunits that vary in number in different species (Table 1). For example, the bc_1 complex in bovine heart contains eight

(A)

Core Subunits	**Prosthetic Group**
Cytochrome *b*	Hemes b_L and b_H
Cytochrome c_1	Heme c_1
Rieske Iron Sulfur Protein	[2Fe2S] Iron Sulfur Cluster

(B)

Source	**Core Subunit**	**Supernumerary Subunit**
Bovine	3	8
Yeast	3	7
Rhodobacter sphaeroides	3	1
Rhodobacter capsulatus	3	0
Paracoccus denitrificans	3	0

Table 1: (A) The three prosthetic groups found in all cytochrome bc_1 complex.

(B) Number of core subunits and supernumerary subunits found in the cytochrome bc_1 complex from different species.

supernumerary subunits (6), in yeast, it contains seven (7), in *Rhodobacter sphaeroides* it has only one (8) and none in *Rhodobacter capsulatus* (9). Although the function of supernumerary subunits is still not fully understood, it is well established that complexes lacking these subunits are less stable and show lower enzyme activity as compared to complexes with supernumerary subunits (7,10). Therefore, it is possible that increased stability and activity of the complex result from the interaction between the redox subunits and the supernumerary subunits.

C. The Q cycle mechanism

The "protonmotive Q Cycle" hypothesis was first proposed by Peter Mitchell (11) to explain the electron transfer and proton translocation in the cytochrome bc_1 complex. Up to this date, several different opinions were projected about the mechanism through which the bc_1 complex operates but the "Q Cycle mechanism" is the generally accepted one because it fully explains the kinetics of reduction of cytochrome c_1 and heme b_H (12).

The two major features of the Q cycle mechanism (Fig. 2) are, first, the existence of two ubiquinone binding site (Qo and Qi sites) and second, the bifurcated reaction at the Qo site (13). In the first turnover of the cycle, one ubiquinol molecule (QH_2) is oxidized at the Qo site on the positive side of the inner mitochondrial membrane where

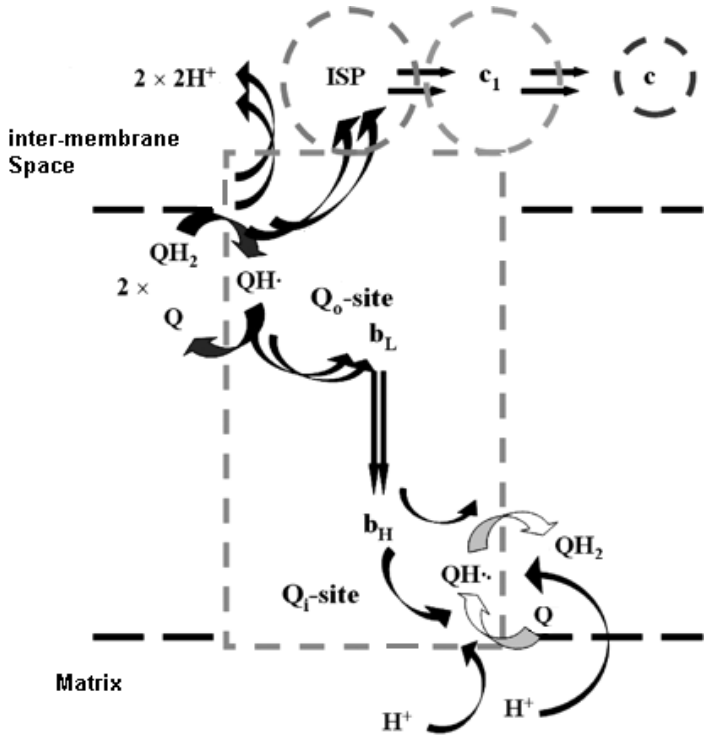

Figure 2: The Q-cycle mechanism showing the reactions catalyzed by the bc_1 complex. The first turnover of the cycle follows the arrow labeled "1" reducing ubiquinone (Q) to ubisemiquinone ($QH^{\cdot}$) and the second turnover of the cycle follows the arrow labeled "2" reducing ubisemiquinone ($QH^{\cdot}$) to ubiquinol (QH_2).

the two electrons diverge with one electron transferred to the high potential chain through 2Fe2S cluster (E_m= 280mV) then heme c_1 (E_m=227mV) to cytochrome c and the second electron transferred to the low potential chain through heme b_L (E_m = -30mV) to heme b_H (E_m =90mV) which reduces ubiquinone (Q) to ubisemiquinone ($QH^{\cdot}$) at the Qi site uptaking one proton from the matrix. In the second turnover of the cycle, the bifurcated electrons at the Qo site follow the same two paths except that heme b_H will transfer the electron to ubisemiquinone, generated in the first turnover, and reduce it to ubiquinol (QH_2), with the uptake of another proton from the matrix. Therefore, in a complete turnover of the cytochrome bc_1 complex, as pointed out in the equation below, one quinone molecule is generated, two cytochrome *c* molecules are reduced and four protons are deposited in the intermembrane space; two protons are deposited upon oxidation of one QH_2 molecule at the Qo site: $QH_2 + 2\ \text{cyt}\ c^{3+} + 2H^+_{(in)} \Rightarrow Q + 2\ \text{cyt}\ c^{2+} + 4H^+_{(out)}$

D. The 3-D structure of the cyt bc_1 complex from bovine heart mitochondria

The three-dimensional structure of the cytochrome bc_1 complex from bovine heart mitochondria, chicken and yeast were determined by X-ray crystallography at a resolution of 2.4 Å (14) , 3.16 Å (15) and 2.3 Å (16), respectively . The bovine structure (Fig. 3) is the most complex one composed of three redox subunits and eleven supernumerary subunits, which fold into a pear-shaped dimeric structure of 130 Å width and 155 Å height. The complex lengthens 38 Å in the intermembrane space from the inner membrane surface housing cytochrome c_1 head and ISP head as well as subunit

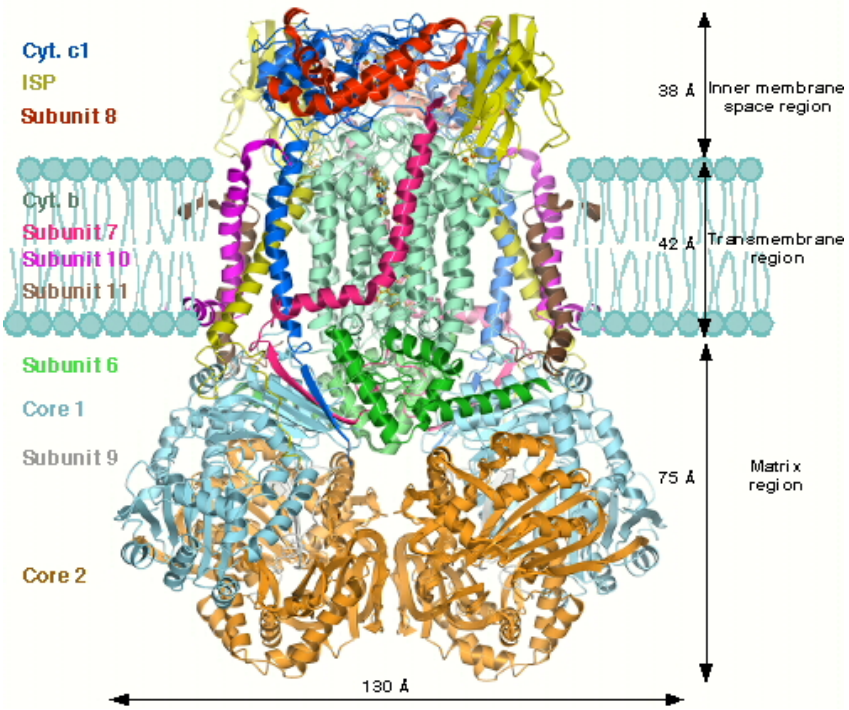

Figure 3. The intertwined dimeric structure of bovine cytochrome bc_1 complex.

VIII. The complex extends 42 Å through the inner membrane consisting of five transmembrane helices from cytochrome b and one helix from each of cytochrome c_1, ISP, subunits VII, X and XI. In the matrix region, the complex extends 75 Å and consists of Core I and Core II subunits, subunits VI and IX as well the C-terminal fragment of ISP and the N-terminal fragment of subunit VII (17). The structural features of the bc_1 complex help understand the mechanism of function of the complex. So far, all structural data support the Q-cycle mechanism, the existence of the bc_1 complex in an intertwined dimeric conformation and the essentiality of the head domain movement of ISP for bc_1 catalysis.

1. The intertwined dimeric structure of the bc_1 complex

Crystallographic observations suggest that the bc_1 complex exists and functions as a dimer with the ISPs of the two monomers intertwined as the ISP tail folds in one monomer and its head domain is in close proximity with cyt *b* and cyt c_1 of the other monomer. To further confirm this observation, mutant bc_1 complexes were generated where two disulfide bonds were introduced between ISP and cyt *b*, one between the head domain of ISP and cyt *b* and the other one between the tail domain of ISP and cyt *b*. SDS-PAGE analysis of this mutant, which shows an adduct protein of molecular weight 128KDa consisting of two cyt *b* subunits and two ISP subunits, confirm that the bc_1 complex exists as a dimer with intertwining ISPs (18).

The functional significance of the dimeric structure of the complex was also implied by studying electron transfer between the two heme b_Ls of the bc_1 complex. The distance between the two heme b_Ls is short enough (21 Å) to allow this transfer and recent studies revealed that disruption of electron transfer between the two b_L hemes increases electron leakage to oxygen resulting in decreased ubiquinol-cytochrome *c* reductase activity (19).

2. Head domain movement of ISP

As revealed by the structure, ISP tail domain (N-terminal) spans the inner membrane and its neck and head domain (C-terminal) are located in the intermembrane space. The head domain movement of ISP between Qo site and cyt c_1 of about 22 Å is presumed critical in the bifurcation of the electron pathway (15). The head domain movement of ISP was further supported by the observation of different [2Fe-2S] cluster positions using different types of Qo inhibitors which either fix ISP head domain in cyt *b* position or leave ISP head domain mobile (20-22). Moreover, several studies were done on a molecular level confirming the crucial role of the head movement in bc_1 catalysis. By increasing the rigidity of the neck domain of ISP by amino acid substitution to Proline (23) or by introducing a disulfide bond in the neck region (24), which decreases the flexibility of the head domain, the enzymatic activity of the bc_1 complex was decreased. In the latter case, activity can be restored only by reducing the disulfide bond. Moreover, a disulfide bond was introduced between the head domain of ISP and cytochrome *b* to

completely immobilize the head domain in the *b*-position. Formation of the inter-subunit disulfide bond completely abolishes the cytochrome bc_1 activity which can be restored to normal activity by reducing the disulfide bond with β-mercaptoethanol (25).

The ISP head domain movement hypothesis may also explain the bifurcated reaction at the Qo site. When quinol is oxidized at the Qo site, one electron is passed to the high potential chain through [2Fe-2S] cluster and the second electron is passed to the low potential chain through heme b_L. The latter thermodynamically unfavorable process could be explained by the head domain movement of ISP; in one model, when the first electron is passed to the iron-sulfur cluster of ISP, ISP head is held in the *b*-position. The iron sulfur cluster being reduced, it cannot accept another electron and only after the second electron is passed to the low potential chain, ISP head moves toward cyt c_1 (20-27). In a different model, proposed by Xiao et. al. (18), ISP head is held in the c_1-position, too far from the Qo site for the second electron to be transferred to it, until the second electron is passed to heme b_L.

E. Photosynthetic bacterium *Rhodobacter sphaeroides* cytochrome bc_1 complex

The photosynthetic bacterium *Rb. sphaeroides* is an anoxygenic purple bacterium that carries out photosynthesis under anaerobic conditions without producing oxygen, in contrast to plants and algae. *Rb. sphaeroides* can also grow under aerobic conditions in the dark when cytochrome bc_1 complex is dispensable for the bacterium growth. Therefore, mutated bc_1 complex that cannot support photosynthetic cell growth can still

be purified. In photosynthetic growth under anaerobic conditions, the cyt bc_1 complex is required for bacterial growth to transfer electrons from quinol to cytochrome c_2. If the cyt bc_1 complex is defective and cannot support photosynthetic growth, cells can be grown under semi-aerobic conditions in the dark where the cyt bc_1 complex is not required because of the presence of quinol oxidase, which transfers the electron directly to oxygen in a cyt bc_1-independent pathway. Under these conditions, intracytoplasmic membrane (ICM) is synthesized from which defective cyt bc_1 complex can be purified and characterized. The ability of *Rb. sphaeroides* to grow under semi-aerobic and anerobic conditions, synthesizing cyt bc_1 complex under either condition, makes it an ideal system for the study of the cyt bc_1 complex. Besides, the bacterial cyt bc_1 complex is a simple protein composed of only four subunits, three catalytic subunits (cyto *b*, cyt c_1 and ISP) similar to their bovine counterparts and one supernumerary subunit, subunit IV. This study focuses on the structure determination of the *Rb. sphaeroides* cyt bc_1 complex and on the interaction between the complex and its electron acceptor, cyt c_2.

F. Importance of this study

The critical importance of cytochrome bc_1 complex has made it a target for numerous antibiotics, fungicides, and anti-parasitic agents. As a result, resistance to these agents has been documented in a wide variety of organisms (28-32). Disorders that are related to defects in the cytochrome bc_1 complex are manifested clinically as

mitochondrial myopathy (33) and exercise intolerance (34). Mounting evidence suggests a correlation between aging and the production of reactive oxygen species from defective cytochrome bc_1 complexes (35, 36). The elucidation of the molecular mechanisms underlying these phenomena requires a combination of experimental approaches and in particular, structural investigations that can provide a molecular framework for further experiments. Because of the importance of the bacterial cytochrome bc_1 complex in functional studies, a high resolution structure has been actively pursued for many years.

In this study, we first report an engineered mutant of *Rb. sphaoeroides* cytochrome bc_1 complex, the SR mutant – SuperReductase - that grows photosynthetically at a similar rate to that of wild type but conspicuously shows higher enzymatic activity and significant increase in protein stability. The discovery of such an active and stable protein provided a breakthrough in the structure determination of *Rb. sphaeroides* cytochrome bc_1 complex, which is discussed at length in the second chapter and compared to its mitochondrial counterpart, providing a vital understanding of the structural-functional relationship of the complex. Ongoing studies related to the structural-functional relationship of the cytochrome bc_1 complex include its interaction with cytochrome c_2, its electron acceptor, which is discussed in chapter three. For this purpose, the soluble part of the bacterial cytochrome c_1, consisting of the head domain, was isolated from the rest of the complex and purified. Interaction studies with cytochrome c_2, using differential scanning calorimetry, were conducted and compared to

the wild type interaction with cytochrome c_2 in the presence and absence of stigmatellin at different salt concentrations.

CHAPTER II

MATERIALS AND METHODS

A. Materials

Cytochrome c (from horse heart) and TMBZ (3, 3', 5, 5'-tetramethyl benzidine dihydrochloride) were purchased from Sigma. N-Dodecyl-*β*-D-maltoside (LM) and N-octyl-β-D-glucoside (OG) were from Anatrace. Ni-NTA gel and Qiaprep Spin Miniprep Kit were from Qiagen. 2, 3-Dimethoxy-5-methyl-6-(10-bromodecyl)-1, 4-benzoquinol ($Q_0C_{10}BrH_2$) was prepared in our lab as previously reported (37).

B. Methods

1. Growth of Bacteria:

E. coli cells were grown at 37ºC in LB medium. *Rhodobacter sphaeroides* BC17 cells bearing pRKD*fbc*FBC$_{6H}$Q (38) plasmid containing the *fbc* genes were grown photosynthetically at 30ºC in an enriched Sistrom medium containing 5 mM glutamate and 0.2% casamino acids. Photosynthetic growth conditions for *Rb. sphaeroides* were essentially as described previously (39). Antibiotics were added to the following concentrations: 125 μg/mL ampicillin, 40 μg/mL Kanamycin sulfate, 10μg/mL tetracycline for *E. coli* and 1 μg/mL for *Rb. sphaeroides*, 100 μg/mL trimethoprim

for *E. coli* and 30μg/mL for *Rb. sphaeroides*.

2. Generation of *Rb. Sphaeroides* expressing mutants of bc_1 complex:

Mutations were constructed by site-directed mutagenesis using the QuickChange system from Stratagene. The double stranded pGEM7Zf(+)-*fbc*FB was used as a template to generate the double mutant S287R(cyt b)/V135S(ISP), referred to as the SR mutant. pGEM7Zf(+)-*fbc*FB was constructed by ligating the *Xba*I-*EcoR*I fragment of pRKD418-*fbc*FBC_{6H}Q (39) into the *Xba*I-*EcoR*I digested pGEM7Zf(+). The primers used to introduce the single mutation V135S in ISP are

V135S-F 5'-CCCACCTCGGCTGCTCGCCGATCGGCGGCGTGTC-3' and

V135S-R 5'-GACACGCCGCCGATCGGCGAGCAGCCGAGGTGGG-3'

The double mutant S287R(b)/V135S(ISP) was constructed using pGEM7fZ(+)-*fbc*FB carrying the single mutant V135S(ISP) as template and S287R(b) primers.

S287R(b)-F 5'-GCGAACCCGCTCCGGACGCCCGCGCACATCG 3' and

S287R(b)-R 5'-CGATGTGCGCGGGCGTCCGGAGCGGGTTCGC-3'

The presence of mutations in ISP and cyt *b* was confirmed by DNA sequencing which was carried out at the Recombinant DNA/Protein Core Facility at Oklahoma State University. Plasmid bearing successful mutations - S287R(b)/V135S(ISP) - was digested with *Xba*I and *EcoR*I and the generated *fbc*FB fragment was purified and ligated to the pRKD418-C_{6H}Q vector, generated from the digestion of pRKD418-*fbc*F$B_{Km}C_{6H}$Q plasmid with *Xba*I and *EcoR*I. The generated pRKD*fbc*FBC_{6H}Q

plasmid bearing the double mutation was chemically transformed to *E. coli* S17 cells. A plate mating procedure (38) was then used to mobilize the plasmid from *E. coli* S17 into *Rb. sphaeroides* BC17.

3. Purification of cyt bc_1 complex from *Rb. sphaeroides*

Chromatophore membranes were prepared as described previously (39) and stored at -80º C in the presence of 20% glycerol until used. Frozen chromatophores were used to prepare cyt bc_1 complex and stored at – 80º C in the presence of 10% glycerol as decribed by Tian *et al* (39)

Protein concentration was determined based on absorbance at 280nm using a converting factor of 1 $O.D_{280} = 0.56$ mg/mL.cm. Cyt *b* (40) and cyt c_1 (41) concentrations were determined spectrophotometrically as published previously.

4. Activity assay of purified bc_1 complex

To assay the activity of cyt bc_1 complex in chromatophore membrane or intracytoplasmic membrane or in purified protein, the preparations were diluted to a final cytochrome *b* concentration of 3 µM with 50mM Tris-Cl, pH 8.0, containing 200 mM NaCl and 0.01% LM. Aliqouts of 2, 4 or 6 µL of the diluted sample was added to 1 mL of assay mixture containing 0.3 mM EDTA, and 100 µM cyt *c* in 100 mM Na^+/K^+ phosphate buffer, pH 7.4. The assays were started by addition of 25 µM Q_2H_2. Activity was determined by measuring the reduction of cyt *c*, which is monitored by the increase

in absorbance at 550 nm in a Shimadzu UV 2102 PC spectrophotometer at 23ºC, using a millimolar extinction coefficient of 18.5. For calculation purposes, the non-enzymatic oxidation of Q_2H_2 in the absence of enzyme under these conditions was subtracted.

5. Generation of *Rhodobacter sphaeroides* cytochrome c_1 truncated mutant C228

The double stranded pGEM7Zf(+)-$C_{6H}Q$ was digested with *Xba*I and *Hind*III to generate the $C_{6H}Q$ fragment which include cytochrome c_1 sequence with a His-tag attached to it and subunit IV sequence. The $C_{6H}Q$ fragment was used as a template in two separate polymerase chain reactions using primers 1 and 1r in PCR reaction 1 and primers 2 and 2r in PCR reaction 2 to delete residues 229-263 in cytochrome c_1 (Fig.1).

Primer 1: 5'- CATGCTCC**TCTAGA**AGGGAAAGGACAGTGA -3'

Primer 1r: 5'- GATCACAGAATTCCTGCTTGCGGGCCATCAG -3'

Primer 2: 5'- GATCGCAGAATTCCATCACCACCACCATC -3'

Primer 2r: 5'- CTCTCCGGATCC**AAGCTT**AAGGTGCAC -3'

Underlined bold sequences in Primers 1 and 2r represent the *Xba*I and *Hind*III restriction site, respectively. Double underlined bold sequences in primers 1r and 2 represent the *EcoR*I restriction site.

Product of PCR reaction 1 was digested with *Xba*I and *Eco*RI while product of PCR reaction 2 was digested with *Hind*III and *EcoR*I. The two generated fragment were then ligated through the *Eco*RI site then ligated to pGEMZf(+) through the *Xba*I and *Hind*III site to generate the plasmid pGEMZf(+)-$C(1\text{-}228)_{6H}Q$.

The deletion of the C-terminal sequence of cytochrome c_1 was confirmed by DNA sequencing which was carried out at the Recombinant DNA/Protein Core Facility at Oklahoma State University. Plasmid bearing successful deletion was digested with *Xba*I and *HindIII* and the generated $C^*_{6H}Q$ (C228Q) fragment was purified and ligated to the pRKD418-*fbc*FB vector, generated from the digestion of pRKD418-*fbc*$FBC_{6H,km}Q$ plasmid with *Xba*I and *EcoR*I. The generated pRKD-*fbc*FBC228Q plasmid bearing the mutation was chemically transformed to *E. coli* S17 cells. A plate mating procedure (38) was then used to mobilize the plasmid from *E. coli* S17 into *Rb. sphaeroides* BC17.

6. Isolation and purification of cytochrome c_1 head domain

Cell pellet was dissolved at a 1:3 ratio with 20 mM Tris-succinate pH 8.0 then passed through French Press twice after the addition of DNase, RNase and 1 mM PMSF. Broken cells were centrifuged at 19K for 15 mns to remove cell pellet and the supernatant was centrifuged at 60K for 75 mns. The collected supernatant was applied to Nickel column equilibrated with 20 mM TrisCl pH 7.4, 1 mM MgSO4. The column was washed first with 20 mM TrisCl pH 7.4, 80 mM NaCl then with the same buffer containing 10mM His then 20 mM His. The proteins were eluted out using FPLC using a histidine gradient from 20 to 200 mM. Fractions of highest purity were combined and concentrated using YM-10 centriprep. Concentrated sample was further purified by FPLC through a Bio 60 molecular sieving column that was equilibrated with 20 mM TrisCl pH 7.4, 80 mM NaCl. Column was washed with same buffer until

protein eluted out. Fractions of highest purity were combined and concentrated using YM-10 centriprep.

7. Isolation and purification of cytochrome c_2

Cytochrome c_2 was purified according to Bartsch (42) with the following additions: the proteins were applied to a Bio 60 molecular sieving column equilibrated with 20 mM TrisCl, pH 7.4, 20 mM NaCl and proteins were eluted with the same buffer. Samples were purified to a Soret/UV ratio (A_{418nm}/A_{280nm}) of > 3.5. The purity was additionally confirmed by SDS-PAGE and concentrated with YM-10 centriprep.

8. Gel electrophoresis, Western Blot preparation and TMBZ heme staining

Sodium dodecyl sulfate - polyacrylamide gel electrophoresis (SDS-PAGE) was performed according to Laemmle (43) using Bio-Rad Mini Protean dual slab vertical cell. Samples were incubated with 10mM Tris-Cl buffer, pH 6.8 containing 1% SDS and 3% glycerol in the presence or absence of 0.4% β-mercaptoethanol for 15 min at 23ºC or 5 min at 60ºC before being subjected to electrophoresis.

Western blot was performed with rabbit monoclonal antibodies against cyt c_1 or against His-tag. The polypeptides separated by SDS-PAGE were transferred to a polyvinylidene difluoride membrane for immunoblotting. Goat anti-rabbit IgG conjugated to alkaline phosphatase or protein A conjugated to horseradish peroxidase

(HRP) was used as second antibody. Color development was done using HRP color development solution.

For TMBZ heme staining, 35 mL of 0.25 M sodium acetate (pH 5.0) were mixed with 15mL of freshly prepared solution of 6.3 mM TMBZ and added to the blotted membrane. The membrane was incubated shaking for 45 min followed by the addition of 1.1 mL 30% hydrogen peroxide. Color development was observed within 5-15 min.

9. Carbon monoxide binding experiment

Carbon monoxide (CO) binding experiment was performed at room temperature. Fully oxidized purified protein (2.5 μM), dissolved in 100mM Tris-HCl (pH 8.0) containing 100 mM NaCl, was first reduced with dithionite and the spectrum was recorded (specR), followed by a short bubbling with carbon monoxide which spectra was also recorded (specR+CO). Carbon monoxide binding was analyzed based on specCO calculation which was calculated from (specR+CO *minus* specR) spectra. No spectral change is expected if no binding of CO is taking place.

10. Differential scanning calorimetry

The experiment was performed using N-DSCII machine. Purified protein (0.55 mL of 15 μM cyt bc_1 complex or 10 μM c-type cytochromes) was first degassed at room temperature for 10 min. Thermoscans from 10 to 90ºC at a rate of 1ºC/min and 2ºC/min were performed during the heating and cooling scans, respectively. Three scans were

recorded, heating-cooling-heating, using the third scan as the baseline for the first scan. CpCalc program was used to calculate Tm values of purified proteins.

11. Determination of redox potential of cyt c_1

The potentiometric titrations of cyt c_1 were essentially done according to the previously published method (46, 47) using the following redox mediators (final concentration): diaminodurol (70 µM), duroquinone (50 µM), Pyocyanine (25 µM), Anthroquinone-2-sulfonic acid (25 µM), Indigo carmine (25 µM), 1,2-naphthoquinone (25 µM), 1,4-benzoquinone (20 µM) phenazine ethosulfate (20 µM), phenazine methosulfate (20 µM). Reductive potentiometric titrations were carried out using dithionite to reduce the ferricyanide oxidized sample and ferricyanide was used for oxidative titration of dithionite reduced sample. All titrations were performed at room temperature using a sealed anaerobic cuvette constantly flushed with argon. The midpoint potential of cyt c_1 was calculated by fitting the redox titration data obtained to the Nernst equation for n = 1.

12. Gel filtration chromatography and co-chromatography

Gel filtration experiments were carried out using Biogel-P60 column at a flow rate of 0.05 ml/min. The column was washed and equilibrated with 20 mM Tris-HCl buffer, pH 7.4 at low ionic conditions and 150 mM NaCl was added at high ionic conditions.

Complex formation was studied by mixing and incubating equimolar amounts of proteins (10 nmoles each) for 20 mns before applying to the column.

13. Crystallization, X-ray diffraction experiment and data processing

The *Rb. sphaeroides* bc_1 purified protein at a concentration of 15 mg/ml, in 50 mM Tris-HCl, pH 7.5, 0.5% β-OG, 5 mM NaN_3, 200 mM NaCl, 200 mM histidine. 10% glycerol, 12% SMC and 10 mM $Sr(NO_3)_2$), was incubated with three to five fold molar excess of stigmatellin and mixed with PEG400 to a final concentration of 8-10%. The mixture was incubated overnight at 4ºC. A small amount of precipitate was removed by centrifugation and the clear supernatant was used for crystallization by vapor diffusion in sitting drops at 15 ºC. Small, red translucent crystals appear within 4-6 weeks. The crystals were frozen in liquid propane and diffraction experiments were performed using synchrotron radiation source at the SER-CAT ID beamline of Advanced Photon Source at Argonne National Laboratory. The X-ray was tuned to a wavelength of 1 Å and crystals were normally exposed for about 2-5 second with an oscillation angle of 0.5°. Diffraction images were collected on a MarCCD-300 detector and were processed with HKL2000 (46). Processing of X-ray Diffraction data was collected in Oscillation Mode. The quality of diffraction of *Rb. sphaeroides* bc_1 crystals were evaluated with the same program.

CHAPTER III

GENERATION, CHARACTERIZATION AND CRYSTALLIZATION OF A HIGHLY ACTIVE AND STABLE CYTOCHROME bc_1 COMPLEX MUTANT

A. Engineering a highly active and stable *Rb. sphaeroides* cyt bc_1 complex

To determine the importance of ISP head domain movement during cyt bc_1 catalysis, several mutants were engineered to increase the interaction between cyt *b* and ISP to immobilize the ISP head domain. Such mutants include introducing one or more disulfide bond(s) to cross-link the two subunits in the membrane domain and to fix ISP head domain in the *b*-position (25). Upon introducing a disulfide bond between ISP head domain and cyt *b*, fixing ISP head in the *b*-position, the cyt bc_1 complex becomes inactive and activity can only be restored upon disruption of the disulfide bond by *β*-mercaptoethanol. Different sets of mutants are being designed to alter the interaction between cyt *b* and ISP to various degrees in order to study the kinetics of electron transfer between c_1 and ISP and to aid with ongoing structure determination of *Rb. Sphaeroides* cyt bc_1 complex. The degree of interaction is manipulated by introducing additional hydrogen bonds between residues of the two subunits that are located in close proximity.

Based on the Bovine mitochondrial structure (47), the distance between Asn263/cyt *b* and Val145/ISP is close enough to allow hydrogen bonding (Fig 4).

A. **B.**

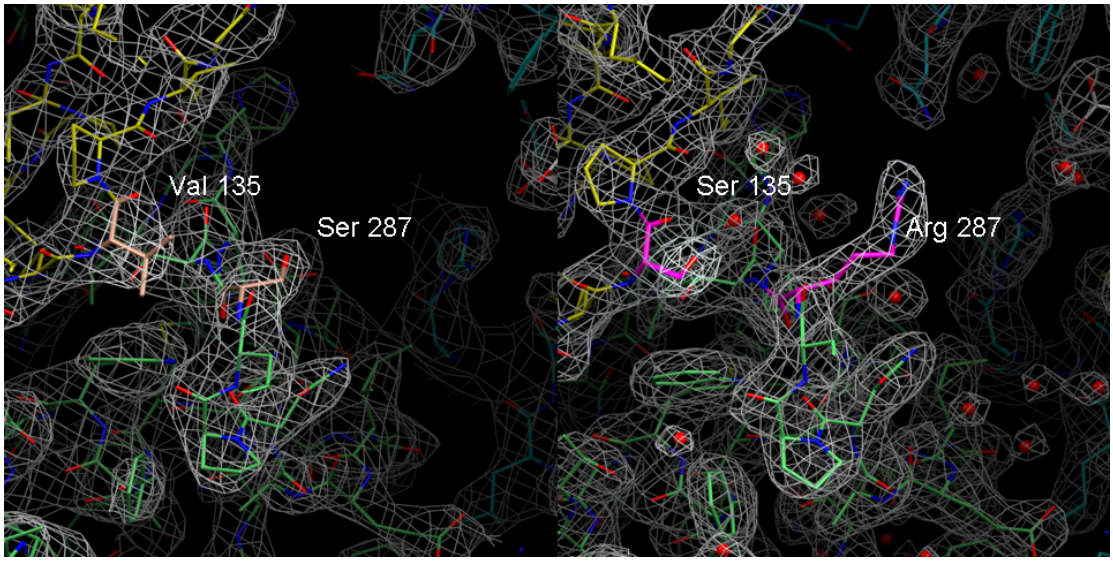

Figure 4: Structure comparison of (A) Wild Type with (B) S287R(b)/V135S(ISP) double Mutant, of *Rhodobacter sphaeroides*

Therefore, the corresponding residues in *Rb. sphaeroides* based on sequence alignment, Ser287 of cyt *b* and Val135 of ISP were mutated to Arg and Ser, respectively. The hydroxyl group of Serine and guanidino group of Arginine are expected to form a hydrogen bond. The cyt bc_1 complex double mutant S287R(b)/V135S(ISP) generated, referred to as the SR mutant, was purified and characterized to reveal the effect of increased interaction between cyt *b* and ISP subunits through potential hydrogen bonding.

B. Characteristics of the SR mutant of *Rb. sphaeroides* cyt bc_1 complex

The purified protein from the double mutant of *Rb. sphaeroides* was subject to detailed studies and compared to the wild type protein. The SR mutant grows photosynthetically at a similar rate to that of wild type. Interestingly, purified chromatophore membranes show a 40% increase in activity as compared to the wild type protein (Table 2). The mutant protein was highly purified with a Soret to UV ratio (A_{418}/A_{280}) of 1.3 compared to a maximum value of 1.2 obtained with purified wild type protein. The mutant protein shows a 40% increase in enzymatic activity as well, compared to the wild type protein. SDS-PAGE analysis (Fig. 5) reveals no difference in subunit composition and concentration between the wild type and the mutant protein. The observation of such a highly active cyt bc_1 complex obviously can not be attributed to a better protein preparation but rather to a higher stability of the complex.

Strain	Mutation	Corresponding residue in Bovine	Ps Growth	Enzymatic Activity		Protein Soret/UV Ratio
				Chromatophore	Purified protein	
WT	-	-	+++	2.0	2.5	1.2
SR	S287R (cyt b) V135S (ISP)	N263 (cyt b) V145 (ISP)	+++	2.8	3.5	1.3

Table 2: Summary of the Wild type and the SR mutant characteristics. Ps Growth (+++) refer to the photosynthetic growth rate of wild type cells. The enzymatic activity is expressed as µmol cyt *c* reduced/min/nmoles cyt *b*.

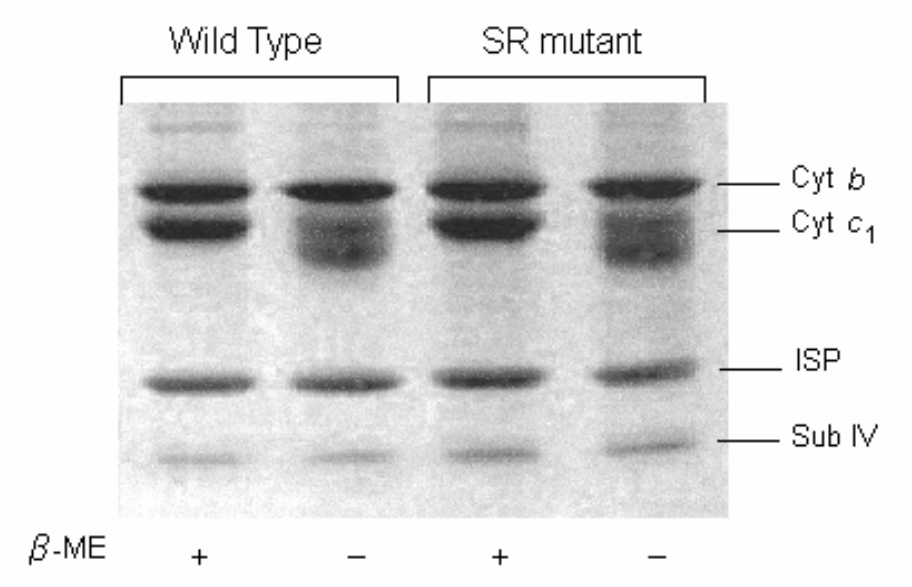

Figure 5: SDS-PAGE analysis of the cytochrome bc_1 complexes isolated from wild type and SR mutant. Samples of proteins were incubated at room temperature under reducing (+ β-ME) or non-reducing (- β-ME) reducing conditions for 15mns before being subject to electrophoresis.

A highly stable protein could be useful to improve the crystallization behavior of *Rb. sphaeroides* cyt bc_1 complex. To study the stability of the protein, the activity of the purified mutant protein was monitored over time, at 25°C and 4ºC, and compared to the wild type activity. As shown in Fig. 6, the activity of the SR mutant decreases at a slower rate than that of the wild type protein. Within 4 days (100 hrs) of incubation at 25ºC, the wild type proteins become inactive whereas the SR mutant proteins still conserve about 50% of activity. Within 12 days (300 hrs) of incubation at 4ºC, the SR mutant proteins conserve 70% of activity as compared to nearly complete inactivation of the wild type protein.

To confirm this conclusion, the purified mutant protein was subjected to a differential scanning calorimetry experiment to analyze its thermo-denaturation temperature. The purified SR double mutant protein showed a 4.3ºC increase in its melting temperature as compared to the wild type protein (Fig. 7). These results confirm that the SR mutant protein is more stable than wild type protein and therefore might be better behaved in crystallization experiments.

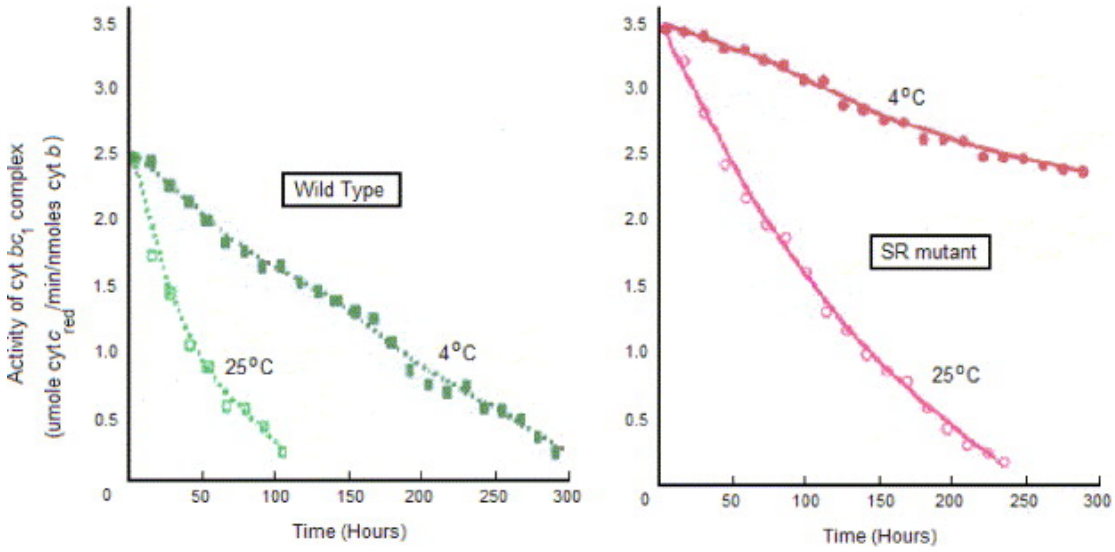

Figure 6: Stability of purified cytochrome bc_1 complex from wild type and SR mutant at 4 °C and 25 °C.

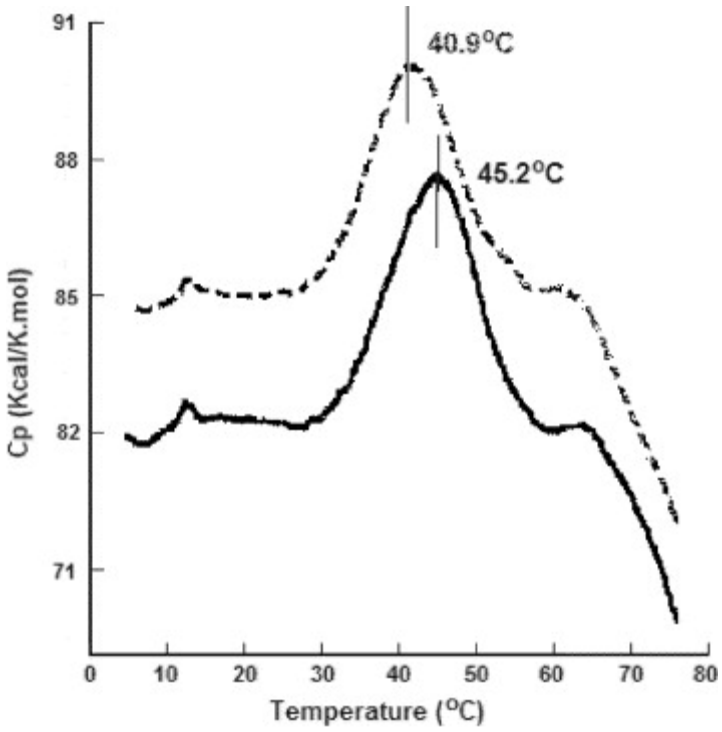

Figure 7: Differential scanning calorimetric study of purified cytochrome bc_1 complex (0.55 mL of 15 μM protein). The thermo-denaturation temperature of the wild type (dashed line) and SR mutant (solid line) cyt bc_1 complex is 45.2 °C and 40.9 °C, respectively.

C. Crystallization Challenges

A lot of effort has been devoted through the years to the crystallization of the wild type cyt bc_1 complex from *Rb. sphaeroides*. Despite of the relative small size and simpler subunit composition as compared to the mitochondrial complex, the bacterial bc_1 complex has been resistant to extensive crystallization efforts as manifested by low quality crystals that diffracted X-rays anisotropically and to low resolution. As prevalent as it is in the field of membrane protein structural biology, the difficulties in crystallizing membrane protein are rooted deeply in the fact that astronomically large number of parameters might affect the protein behavior in, and thus the outcome of, a crystallization experiment. One of these parameters and with no doubt an important one is the stability of the protein. Since the crystallization process often involves a prolonged incubation period, the observed enhancement in stability of the mutant protein is thought to offer an appealing system to screen for better conditions for *Rb. sphaeroides* cyt bc_1 crystals. Indeed, the SR mutant was crystallized in the presence of stigmatellin, which further stabilizes the structure to help resist long incubation periods, at 15ºC in several different crystal forms. Small, red translucent crystals were observed within 4-6 weeks. More importantly, the mutant *Rb. sphaeroides* cyt bc_1 preparation allowed us to identify conditions that produced crystals diffracting X-rays uniformly to 2.4Å resolution. A detailed description of the structure determination and analysis of *Rb. sphaeroides* cyt bc_1 complex is discussed in details in the next chapter.

CHAPTER IV

STRUCTURE DETERMINATION OF *RHODOBACTER SPHAEROIDES* CYTOCHROME bc_1 COMPLEX

A. Introduction

Significant advances in elucidating architectural features of the cytochrome bc_1 complex have been made by crystal structure determinations of the mitochondrial bc_1 complex (47-50) and b_6f complex from a bacterium (51) and an alga (52). In particular, crystal structures of mitochondrial bc_1 in complex with various bc_1 inhibitors provide important mechanistic insights (53-60), leading to a significant increase in the number of experimental studies and analyses of this enzyme. However, most recent functional investigations have been conducted with bacterial bc_1 complexes, especially those of non-oxygenic photosynthetic purple bacteria such as *Rb. sphaeroides* and *Rb. capsulatus* (*Rc*). These bacterial systems contain simpler bc_1 complexes consisting of either three (*Rc*) or four (*Rs*) subunits whose sequences have remained close to their mitochondrial counterparts. Site-specific mutants can be readily prepared and tested and chromatophore vesicles are easy to isolate in large quantities. Because of the importance of bacterial bc_1 in functional studies, a high-resolution structure has been actively pursued for many years. The crystal structure of the bc_1 complex from *Rb. capsulatus* reported at 3.8Å

resolution represented the first step toward this goal (61), though it lacks sufficient resolution of structural details that distinguish the bacterial form from the mitochondrial one. In this chapter, the crystal structures of the wild type and SR mutant bc_1 complex from the *Rb. sphaeroides* with bound inhibitors ranging in resolution from 3.1 to 2.4Å are reported.

B. Structure determination and overall structure of *Rb. sphaeroides* cyt bc_1 complex

The presence of the Q_P site inhibitor stigmatellin, the use of the amino acid histidine and a mixture of β-octyl glucopyranoside (β-OG) and sucrose monocaprate (SMC) are important for obtaining high quality crystals. A batch of *Rb. sphaeroides* SR mutant appeared to be particularly suitable for growing well-behaved crystals, which diffracted x-rays to 2.35Å resolution. Three bc_1 dimers occupy the crystallographic asymmetric unit (ASU). The wild type enzyme crystallizes with two dimers per ASU and diffracts x-rays to 2.6Å resolution. Surprisingly, only the three core subunits are present in both wild type and mutant *Rb. sphaeroides* cytochrome bc_1 crystals; apparently, subunit IV was lost upon crystal formation. The assembly of the three-subunit bacterial bc_1 complex (Fig. 8) resembles closely that of the corresponding subunits in bovine mitochondrial bc_1 complex (47) and the remarkable conservation in architectural features

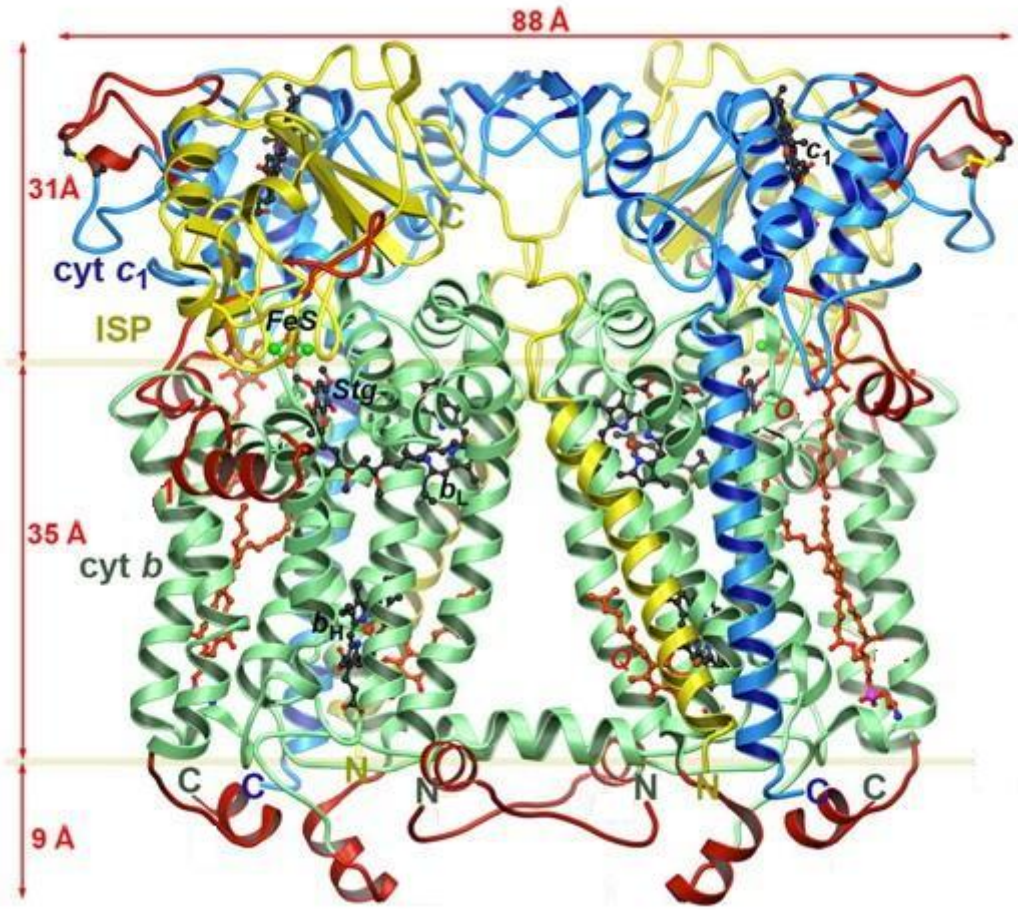

Figure 8: Structure of *Rhodobacter sphaeroides* cytochrome bc_1 complex. The subunits are colored as follows: *green*, cyt *b*; *blue*, cyt c_1, and *yellow*, ISP. Insertions and extensions are in *red*. Heme groups, *2Fe2S*, stigmatellin and ubiquinone are shown as *stick models.*

not only pertains to a single monomer but also to an assembled homodimer. The deviation between the cytochrome *b* dimers of *Rb. sphaeroides* and bovine bc_1 complex is less than 1.1 Å for C_α atoms. Consequently, the distances between prosthetic groups are virtually identical, implying functional conservation. As in mitochondrial bc_1 complex, the extrinsic domain of the iron-sulfur protein subunit in *Rb. sphaeroides* crosses over, connecting one molecule of cyt *b* to the adjacent one. In contrast to the seven or eight supernumerary subunits in mitochondrial enzymes, *Rb. sphaeroides* cytochrome bc_1 complex has only one. Thus, it has been speculated that supernumerary subunits represent functional or structural equivalents of the insertions, extensions, and deletions found in the sequences of the catalytic subunits of the bacterial bc_1 complex (62).

C. Structure of the cytochrome *b* subunit

The cyt *b* subunit of *Rb. sphaeroides* cytochrome bc_1 complex has eight membrane spanning helices named A to H, forming two helical bundles (A-E and F-H) (Fig. 9). The two heme groups, b_L and b_H, reside within the first bundle. Extra membranous loops connect pairs of transmembrane (TM) helices and the AB, CD, DE and EF loops are longer than 20 residues. The quinol oxidation site (Q_P, Q_0) near the periplasmic side of the membrane and quinone reduction site (Q_N, Qi) on the opposite side can be identified with bound stigmatellin and antimycin, respectively.

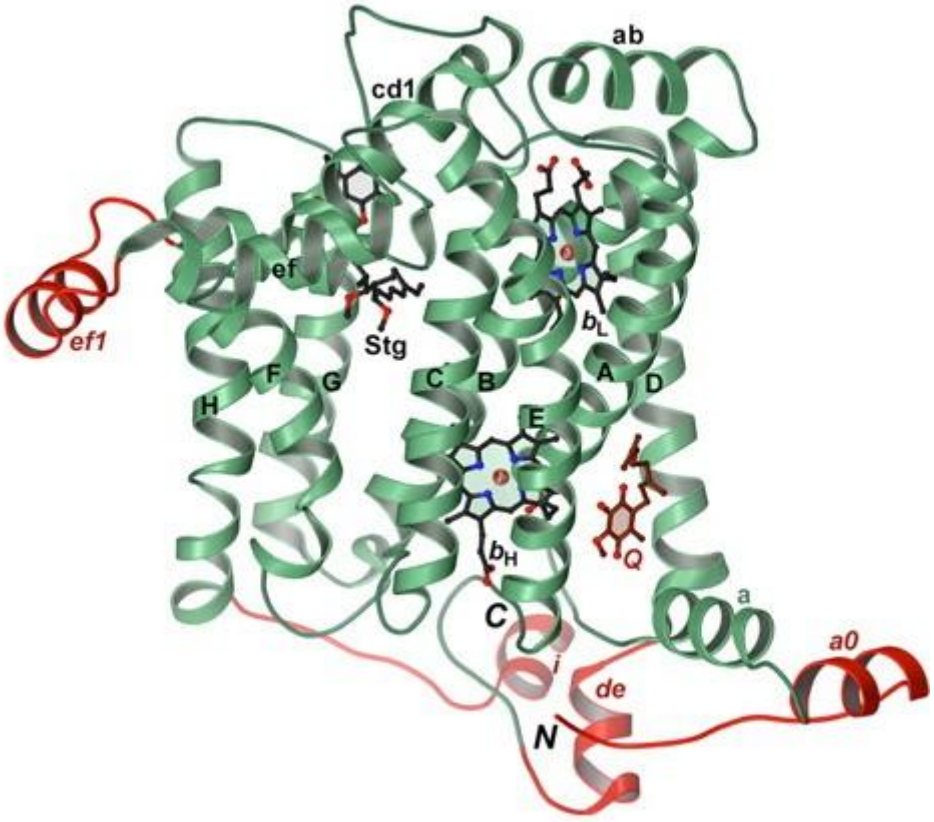

Figure 9: Ribbon diagram of the cytochrome *b* subunit with labeled TM helices and connecting loops. The insertions, as compared to the bovine counterpart, are shown in red.

When compared with structures of mitochondrial cytochrome bc_1 complex, the bacterial *cyt b* features two terminal extensions and two major insertions. The N- and C-terminal extensions are 22 and 29 residues long, respectively. Both contain helices named a0 and i, respectively. One insertion (de helix) is in the cytoplasmic DE loop and another (ef1 helix) inserts after the ef helix on the periplasmic side.

D. Structure of the cytochrome c_1 subunit

The cytochrome c_1 subunit folds in a manner similar to that of its mitochondrial counterpart, having a C-terminal TM helix (Fig. 10A) and featuring the Cys^{37}-*X*-*X*-Cys^{40}-His^{41} motif characteristic for *c*-type cytochromes with the heme iron atom being coordinated by the side chains of His^{41} and Met^{186} as 5th and 6th ligand, respectively. The heme group is located and positioned identically to that of mitochondrial enzymes. Crystals of *Rhodobacter sphaeroides* cytochrome bc_1 complex grown in the presence of strontium ions (Sr) revealed a metal ion-binding site on cyt c_1 (Fig. 10B) which is not present in mitochondrial bc_1 but appears to be conserved in photosynthetic bacteria (Fig. 11). The strontium ion is accessible from the periplasm and coordinated by side chains of Asp^8, Glu^{14}, and Glu^{129} as well as by the backbone carbonyl oxygen atom of residue Val^9 in a distorted octahedron. To our knowledge, this metal ion-binding site has not been described previously and its possible physiological role is currently under investigation.

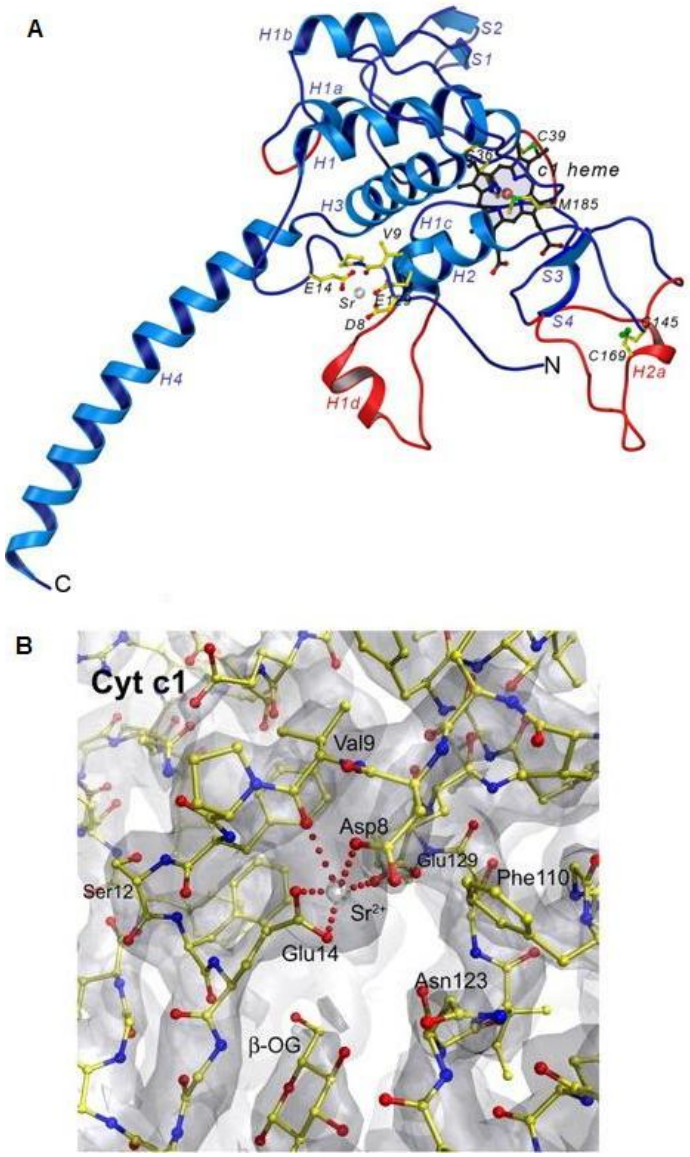

Figure 10: Structure of *Rb. sphaeroides* cytochrome c_1 subunit. (A) Ribbon structure showing extra-fragments in red. (B) Residues important for Sr (metallic sphere) binding are drawn in stick models with carbon atoms in *yellow* and oxygen in *red*.

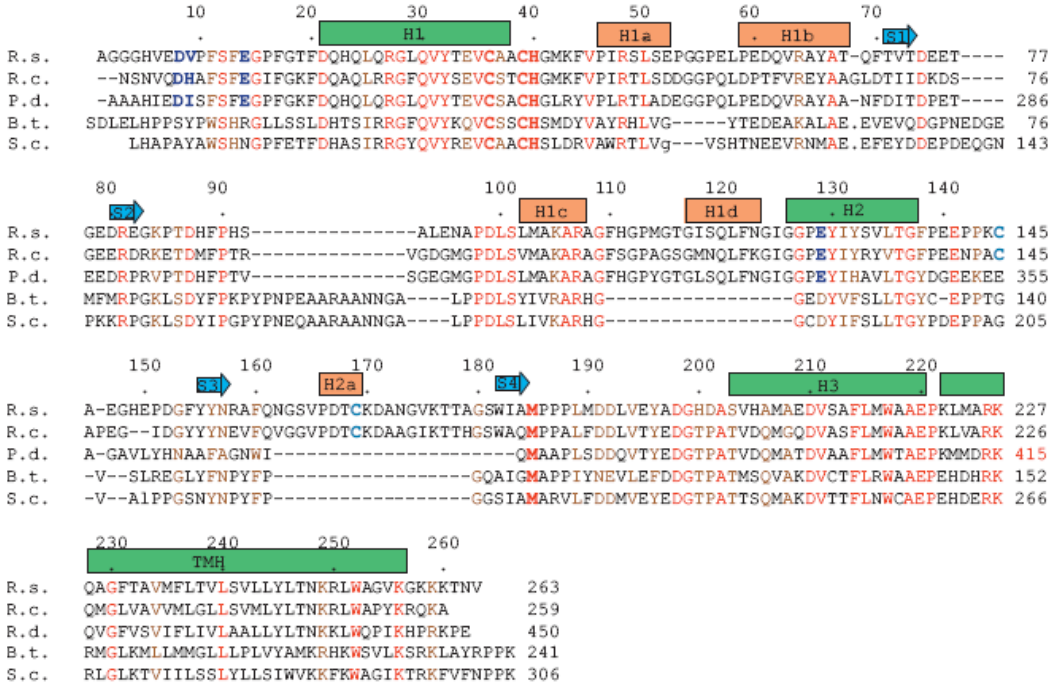

Figure 11. Structure-based sequence alignment of *Rb. sphaeroides* cytochrome c_1. Secondary structure elements are shown as *boxes* for α-helices and *arrows* for β-strands. *Green boxes* and *blue arrows* indicate shared secondary structure elements between bacterial and mitochondrial bc_1, whereas those colored in *orange* are found in bacteria only. Residues that are ligands to the heme are *red* in *bold face*. Residues that are fully conserved in the alignment are shown in *red*; those having conserved changes are *brown*. The sequences are *R.s.* (*R. sphaeroides*), *R.c.* (*R. capsulatus*), *B.t.* (*B. taurus*), *S.c.* (*S. cerevisiae*) and *C.r.* (*C. reinhardtii*).

E. Structure of the Iron-sulfur protein subunit

The ISP subunit has a C-terminal periplasmic head domain (extrinsic domain, ISP-ED), which connects through a flexible hinge region to its N-terminal TM helix (Fig. 12). The ISP-ED is predominantly a β-structure consisting of three β-sheets arranged in three parallel layers with the *2Fe2S* cluster located at the apex of the ISP-ED between the 2nd and 3rd β-sheet. The conserved ADV motif in the hinge region adopts an α-helical (HA) conformation, unlike the random coil secondary structure of bovine bc_1. One insertion with respect to the bovine sequence is located between Thr^{96} and Ala^{109}, filling a surface depression that would otherwise exist between β-sheets 2 and 3.

F. Insertions and deletions in *Rb. sphaeroides* cytochrome bc_1 relative to the mitochondrial cytochrome bc_1 complex

When sequences of mitochondrial bc_1 and bacterial bc_1 complexes are compared, the latter often possesses more insertions than deletions. Remarkably, the insertions occur only on or near the periplasmic or cytoplasmic side and not within the transmembrane region (Fig. 8). An understanding of the functions of these additions or deletions may provide insight into the evolutionary process that transformed the bacterial enzyme into its mitochondrial equivalent. Characteristic of this process is the addition of

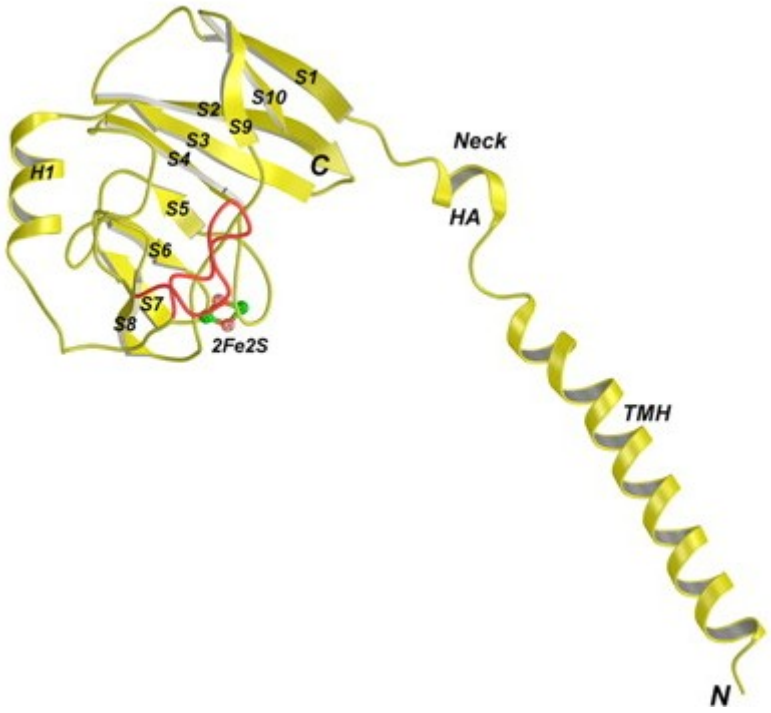

Figure 12: Ribbon structure of *Rb. sphaeroides* Iron-sulfur protein (ISP). Extra-fragment shown in red.

supernumerary subunits that possibly provide structural stability and functional integrity to the enzyme (3).

1. Insertions in cytochrome *b*

Cyt *b* of *Rb. sphaeroides* cytochrome bc_1 complex is 66 residues longer than its bovine mitochondrial equivalent. As seen in its structure (Fig. 9), bacterial bc_1 has extensions at both termini (a0 and i helices), a helical insertion between the D and E helices (de helix) as well as an insertion between the ef-loop and the F helix (ef1 helix). In the structure, the C terminus of cyt *b* is visible up to residue 430, consistent with the observation that deletion of the last 15 residues does not affect the function of the bacterial bc_1 complex (62). Except for the ef1 helix, all extensions and insertions are located on the N-side of the membrane (Fig 9), which likely function to maintain the structural integrity of the quinone reduction site by preventing potential electron leakage and by safeguarding channels for proton influx (59). Indeed, without the supernumerary subunits, especially core1 and core2, the heme b_H (and with it the Q_N site) of the mitochondrial cyt *b* is only weakly shielded from the aqueous matrix by a thin layer of protein side chains. In contrast, the Q_N site of *Rb. sphaeroides* cytochrome bc_1 complex is well protected by an additional layer consisting of the de-helix insertion and the two terminal extensions. The location of the de-helix permits interaction with its own C-terminal extension and with the end of the N terminus from the neighboring cyt *b* through a network of hydrogen bonds. The a_0-helix reaches to the cyt *b* of its symmetry mate and

forms a pair of salt bridges between Arg^{22} and Glu^{126} of the symmetry-related cyt *b* and a number of hydrogen bonds as well as van der Waals interactions (Figs 8 and 9). Mutational studies have shown that C-terminal truncations as far as residue 421 lead to increasing detergent sensitivity, loss of ISP and subunit IV during purification and lowering the potentials of both heme groups, leading to eventual inactivation of *Rb. sphaeroides* cytochrome bc_1 complex (62). The structure qualitatively explains these observations by demonstrating the interaction of the C terminus of cyt *b* (via the i helix) with the C terminus of cyt c_1 (indirectly to the N terminus of the ISP) and with the de-helix, which is in close proximity to the b_H heme.

On the periplasmic side, there is one large insertion of 18 residues (310-327) between Pro^{285} and Asn^{286} of mitochondrial cyt *b* containing the ef1-helix, which protrudes from cyt *b* laterally and runs parallel to the membrane surface (Fig 8). This insertion occurs only in bacteria. However, it is functionally important, as the point mutation S322A or deletion of residues 309-326 significantly lowers the enzyme activity (63). The ef1-helix may play an important role in lipid binding and it also enhances crystal contacts through aromatic stacking interaction between Trp^{313} of adjacent cyt *b* subunits.

2. Insertions and deletions in cytochrome c_1

The structure-based sequence alignment (Fig. 11) shows that cyt c_1 of *Rb. sphaeroides* cytochrome bc_1 complex has undergone both insertions and deletions relative to mitochondrial complexes. Apart from the two small insertions in the *Rb. sphaeroides* cyt c_1 after Glu^{52} (4 residues) and Ala^{146} (3 residues), there is one large insertion between Gly^{109} and Gly^{127}. It features a short helix (H1d) that protrudes from cyt c_1 into the lipid bilayer sealing off a compartment between cyt c_1 and cyt *b* (Fig. 8 and 10). In mitochondrial cyt bc_1 complex, the absence of this insertion creates a niche at the interface between the end of the Helix E of cyt *b* and cyt c_1. A possible function of this insertion may relate to lipid binding. The only insertion in cyt c_1 that may replace the function of a supernumerary subunit is the 18-residue insertion starting at position 162, which is spatially close to the head domain of ISP (Fig. 13). Containing a short helix H2a, this region features a stabilizing disulfide bridge (Cys^{145}-Cys^{169}), whose existence is in agreement with previously published studies (64), discussed at length in my Masters' Thesis. Approaching the ISP-ED within ~ 8Å (C_α distance from cyt c_1 Asn^{173} to ISP Asp^{143}), this insertion presumably functions as an extended arm to limit the motion of the ISP-ED (Fig. 13). However, the intrinsic flexibility and extent of solvent exposure renders it susceptible to proteolytic attack and, conceivably, places it in an evolutionarily disadvantageous position, possibly leading to the replacement of its function by the supernumerary subunit VIII in mitochondrial enzymes.

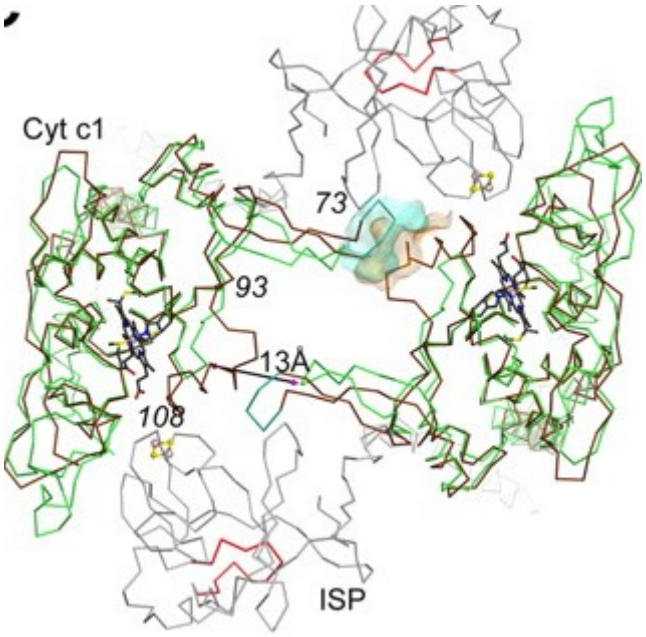

Figure 13: Stereo view of a superposition of Cα traces of *Rb. shaeroides* (*green*) and bovine (*brown*) cyt c_1 looking down the periplasmic side into membrane bilayer. Also shown is the *Rb. sphaeroides* ISP (*gray*) in the hypothetical c_1 position. The insertions are shown in *Red*.

Compared with mitochondrial cyt c_1, two large deletions, near residues Thr^{77} and Ser^{92}, respectively (Fig. 11) result in the loss of bridging interactions between the two cyt c_1 subunits within the dimer (Fig. 13). The absence of these contacts in *Rb. sphaeroides* bc_1 complex creates a large continuous groove (13 Å wide) on the P-side surface. Beyond possible functional implications, the closure of the gap improves stability around the heme group in mitochondrial cyt c_1.

3. Insertions in the Iron-sulfur protein (ISP)

Structure-based sequence alignment shows one insertion in the sequences of *Rb. sphaeroides* ISP (Fig. 12). This insertion (residues 97-108) is located on the surface of ISP-ED distal to cyt c_1 and stays 20-25 Å away from the *2Fe2S* cluster as predicted (65); it forms a globular structure containing three β-turns and one inverse γ-turn. There is an intricate network of interactions employing both main chain and side chain atoms, suggesting a stabilizing role for this insertion. Disruption of this network of interactions by more than one point mutation led to the loss of the ISP subunit in the complex (65). From a morphological point of view, the insertion 97-108 in *Rb. sphaeroides* bc_1 complex help maintain the globular shape of the ISP-ED as compared with its mitochondrial homologues.

G. Fate of the Subunit IV

Purified *Rb. sphaeroides* cytochrome bc_1 complex, both wild type and SR mutant, contains one additional 14.4-kDa subunit (subunit IV), which has been shown to enhance the activity of the core subunits by 68% (66) but is not essential for the function of the complex or the survival of the organism. The same observations have been made about the non-essential 6-kDa subunit in *Rhodovulum sulfidophilum* bc_1 (67). In fact, many of the known bacterial forms of bc_1, including *Rhodobacter capsulatus* and *Paracoccus denitrificans*, contain only the required three core subunits, cyt *b*, cyt c_1 and the ISP. In the crystal structure, however, subunit IV is missing from the complex, indicating that the crystallization medium (including PEG400, detergents, etc.) must have caused the detachment of subunit IV. A SDS-PAGE gel revealed the presence of subunit IV in solution, but showed no detectable amount in crystals. It is not uncommon to lose a supernumerary subunit during crystallization of mitochondrial bc_1 complexes (50,60). To test whether subunit IV is indirectly required for the crystallization of *Rb. sphaeroides* bc_1 complex, we purified the Δ-subIV mutant (68) and subjected it to the same crystallization conditions. Crystals grew readily and diffracted x-rays to 3.1Å resolution. The structure could be readily solved and refined (Data not shown), demonstrating that the subunit IV is not required for crystallization.

Atomic coordinates of the redefined inhibitor-bound *Rb. sphaeroides* bc_1 complex structures have been deposited in the Protein Data Bank with accession codes: 2QJP (wild type, stigmatellin and antimycin), 2QJY (double mutant, stigmatellin), 2QJK (double mutant, stigmatellin and antimycin).

CHAPTER V

PURIFICATION AND CHARACTERIZATION OF *RHODOBACTER SPHAEROIDES* CYTOCHROME C_1 HEAD DOMAIN AND INTERACTION STUDIES WITH CYTOCHROME C_2

A. Introduction

1. Background

The *Rb. sphaeroides* cytochrome c_1 subunit, the site of interaction between the cyt bc_1 complex and cyt c_2, is composed of 263 amino acids with a theoretical molecular weight of 30.5KDa but is identified as a protein with a molecular weight of 34KDa on SDS-PAGE. Mature cyt c_1 houses a type *c* heme through the conserved CXXCH heme-binding consensus sequence in the head domain. The binding interaction between cytochrome *c* and cytochrome c_1 has always been thought to be primarily electrostatic (69-72). The effects of ionic strengths on the complex formation between cyt *c* and cyt c_1 have been consistent with the role of electrostatic interaction in the complex formation and stabilization. Evidence for a docking model involving charged residues was obtained by chemical modifications and site-directed mutagenesis of the lysine amino groups to negatively charged groups on the interface of cyt c_2, which resulted in decreased binding

between cyt c_2 and the cyt bc_1 complex (71-73). These results supported the involvement and importance of the positively charged residues in cyt c_2 in the interaction with the cyt bc_1 complex. In a complementary study, a water-soluble carbodiimide was used to show that specific carboxylate groups on cyt c_1 are involved in binding cyt *c* (74). Two acidic regions, rich in glutamate and aspartate residues, in mitochondrial cyt c_1 were implicated in the formation of the complex with cyt c, which were found to be conserved amongst most bacterial cyt c_1 sequences and thus believed to be directly involved in binding cyt c_2. In an independent study, the reaction of bovine heart cyt c_1 with ruthenium-cyt *c* derivative by flash photolysis showed a progressive decrease of electron transfer rate constant within the complexes with increasing salt concentration indicating a dissociation of the complex at increasing ionic strength (75). The X-ray structure of beef and yeast cyt bc_1 complex reveal the presence of acidic residues on the cytoplasmic side of cyt c_1 head domain which are believed to be cyt *c* docking site (16, 47). However, the structure of the complex between cyt *c* and the stigmatellin-bound cyt bc_1 complex from yeast, solved at 2.97º, revealed the binding of cyt *c* to one of the two possible cyt c_1 binding sites of the homodimeric complex, stabilized mainly by hydrophobic interactions (76, 77). A more recent study using ruthenium-labeled cyt *c* derivative to study electron transfer with the cyt bc_1 complex showed that the complex between cyt *c* and bovine cyt bc_1 complex dissociates at a much lower ionic strength than the corresponding complex between yeast cyt *c* and yeast cyt bc_1 complex and that it is possible that the yeast cyt *c*:cyt bc_1 complex assumes a different orientation in solution than in the crystal (78). Hence, the interaction

between cyt c_1 and cyt c_2 remains controversial and reported data raises the question of the effect of stigmatellin on the structure of cyt bc_1 and thus the interaction between cyt c_1 and cyt c_2.

2. Purpose of study

To better understand the reaction mechanism of photosynthetic electron transfer, it is crucial to elucidate the molecular structure of its components and the reaction of complex formation amongst them. Previously published results raise many questions about the physiological nature of the interaction between cyt c_1 and its electron acceptor cyt *c* and the effect of stigmatellin binding to the cyt bc_1 complex on complex formation with cyt c_2. To study such interaction without ambiguity, the cyt c_1 head domain from *Rb. sphaeroides* cyt bc_1 complex was isolated and purified from an engineered truncated mutant, C228. The full length cyt c_1 has been previously isolated by our group (79) and characterization of the purified subunit showed identical properties to mammalian cyt c_1 revealing the conservation of structure and function of cyt c_1 upon isolation from the cyt bc_1 complex. The purified cyt c_1 head domain was used for comparative interaction studies, using differential scanning calorimetry (DSC), between cyt c_2 and each of the cyt bc_1 complex and cyt c_1 head domain, in the presence and absence of stigmatellin, at different ionic strength. In this chapter, we report the different attempts to isolate the head domain of cyt c_1 providing an elaborate method to purify an intact and fully functional cyt c_1 head domain. The nature of interaction between cyt c_1 head domain and cyt c_2 is

discussed at length revealing the effect of salt and stigmatellin on the affinity and nature of binding between the two cytochromes.

B. Construction and isolation of cytochrome c_1 head domain

Several attempts to construct single mutants generating the cyt c_1 head domain by either introducing a stop codon at the neck of cyt c_1 following Q228 or by mutating Q228 itself to a stop codon, as reported by Konishi, K. et al (80), have repeatedly failed due to the reversion of the mutant to wild type during semi-aerobic growth. An additional attempt to isolate the head domain was done by a triple mutation of L223I, M224D, A225G of LMAR sequence to generate Factor Xa cleavage consensus sequence IDGR. The generated mutant can grow photosynthetically at a comparable rate to wild type but the purified protein has an enzymatic activity of 1.0 μmol cyt *c* red/min/nmoles cyt *b* which constitutes 40% of wild type activity. Beside the significant loss in activity, the attempt to digest the bc_1 complex with Factor Xa was unsuccessful, most likely due to the inaccessibility of Factor Xa to the introduced IDGR site. The only successful way to isolate the soluble head domain is to engineer a mutant excluding the tail domain of cyt c_1 and attaching the histidine tag directly to the neck region. Due to the length of the tail domain of cyt c_1 (229-263), a deletion mutagenesis is unfeasible. Therefore, PCR was used to amplify the required fragments to express the cyt c_1 head domain, ending at residue 228, with an attached his-tag and thus generating the C228 mutant.

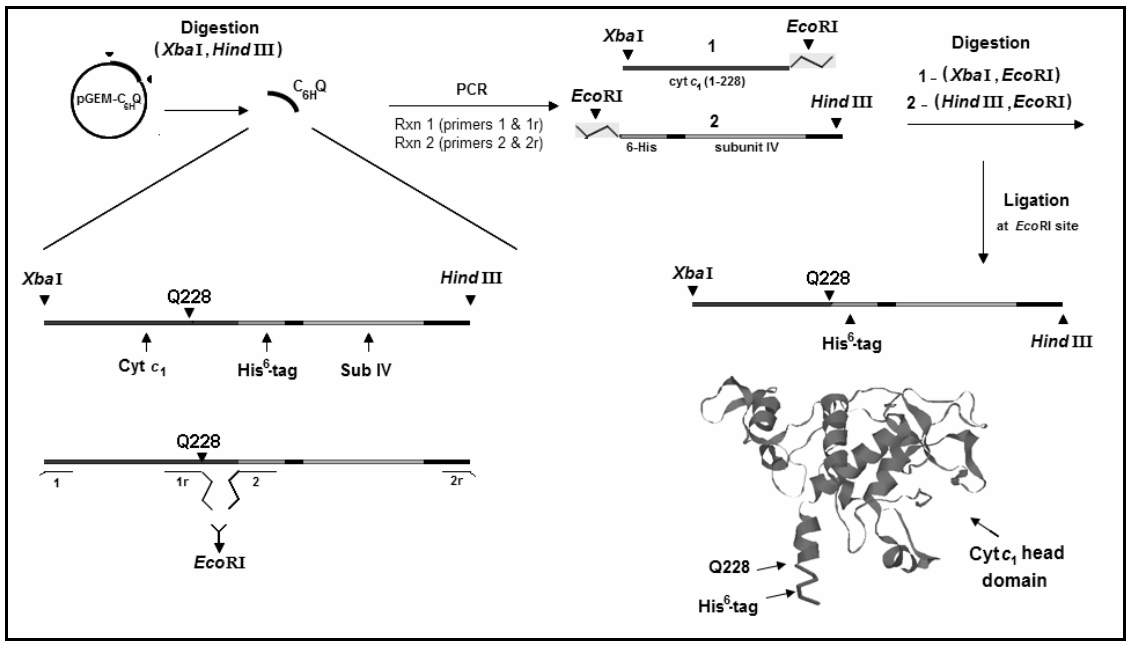

Figure 14: Engineering of cyt c_1 truncated C228 mutant consisting of His-tagged cyt c_1 head domain. PCR reaction-1 product contains cyt c_1 fragment consisting of residues 1 to 228 and PCR reaction-2 product contains the 6-His tag followed by a stop codon and subunit IV. Upon ligation of the two digested products with the indicated restriction enzymes, the generated insert fragment contains a His-tagged cyt c_1 head domain sequence (1-228) and subunit IV which is then ligated to the expression vector pRKD418-*fbc*FB as described in Materials and Methods.

Figure 14 illustrates the steps followed to generate the truncated C228 mutant and a detailed description of protein expression in *Rb. sphaeroides* and protein purification is included in the Materials and Methods section. In summary, cell pellet of C228 mutant is broken, using French press, and centrifuged at 60K for 75mns. When starting with 50 g of cells, the *c*-type cytochrome content in the collected supernatant, after ultracentrifugation, is on average 1.46 μmoles (Table 3). The collected supernatant is then applied to a nickel column. Around 88% of *c*-type cytochrome content is recovered in the effluent, which contains mostly cyt c_2 as well as some cyt c_1 head domain that did not bind to the column. After three washing steps, the proteins are eluted out using a histidine gradient from 20 to 200mM. Fractions of highest purity are combined and concentrated using YM-10 centriprep. A total of around 145nmoles of cyt c_1 head domain, which constitute 10% of the original *c*-type heme content, is recovered through nickel column with a Soret/UV ratio of 2.2. Concentrated sample is further purified by FPLC through a Bio 60 molecular sieving column. The protein were applied to the column and washed out at a rate of 0.05ml/mn. Fractions of highest purity, with a Soret/UV ratio of 4.2 are combined and concentrated using YM-10 centriprep and centricon. A total of 105nmoles of cytochrome c_1 head domain protein, which constitute 7.0% of the original *c*-type cytochrome content, is recovered from 50g of cell pellet with a Soret/UV ratio of 4.2 showing as a single band on SDS-PAGE (Figure 15).

Treatment	Volume (ml)	c-type heme protein		cyt c_1 Head Domain			
		Concentration (µM)	Total (nmoles)	Concentration (µM)	Total (nmoles)	Purity	Yield
Supernatant	130	11.2	1456	–	–	N/A	100%
Ni-Column effluent	135	9.5	1282	–	–	N/A	N/A
Ni-Column eluent	0.7	210	145	210	145	2.2	10%
Gel filtration eluent	0.3	350	105	350	105	4.2	7%

Table 3: Isolation and purification of cyt c_1 head domain from C228 mutant. The purity of the cyt c_1 head domain the Soret/UV ratio of $A_{417}/A_{280.}$ A detailed description of the stepwise isolation and purification of the head domain is included in the Materials and Methods section. The data given in this table is averaged from three batches of C228 mutant.

C. Properties of cytochrome c_1 head domain

The isolated truncated cyt c_1 constitutes the soluble head domain of the cyt c_1 subunit, which comprises residues H1 to Q228 with an attached his-tag and has a theoretical molecular weight of 28KDa. The soluble head domain was purified, as described in the previous section, to a Soret/UV ratio of 4.2 showing as a single band, of an apparent molecular weight of 30KDa on SDS-PAGE, under reducing conditions (Figure 15A). Under non-reducing conditions, cyt c_1 head domain follows the pattern of the wild type cyt c_1 showing as a smear band, which indicates the presence of the covalently bound heme in the purified domain, further confirmed by TMBZ heme staining (Figure 15B). The head domain has similar spectral properties as the wild type cyt c_1 (Figure 16). The soret band wavelength for oxidized and reduced cyt c_1 head domain is 410nm and 417 nm, respectively. Its α-band wavelength is 552nm with an extinction coefficient of 17.5 $mM^{-1}.cm^{-1}$, which is comparable to the wild type full-length subunit. Reducibility by ascorbate implies a stably functional head domain, which was further confirmed by a negative reaction with carbon monoxide (Figure 17) and by its midpoint potential, determined to be 220mV which is comparable to the wild type cyt c_1 potential of 235mV (Figure 18).

The characteristics of cyt c_1 head domain are similar to the wild type full length cytochrome c_1 which makes the domain suitable for in vitro interaction studies with its

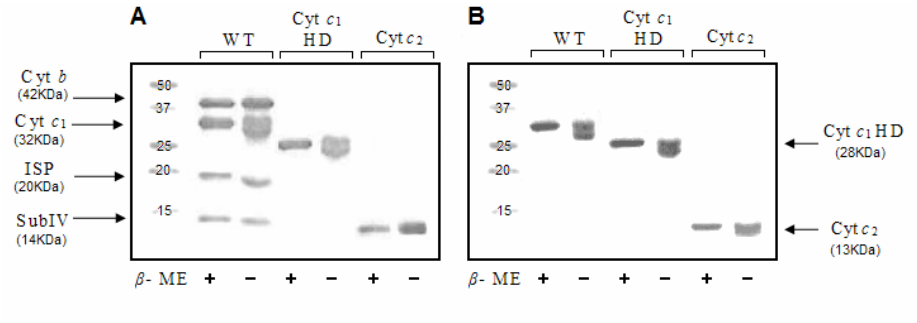

Figure 15: (A) SDS-PAGE and (B) TMBZ heme staining analysis of the cyt c_1 head domain compared to wild type cyt c_1 from the cyt bc_1 complex and cyt c_2. Samples of protein (70pmoles) were incubated in the presence of β-mercaptoethanol as reducing agent at room temperature for 15min before being subjected to SDS-PAGE as described in the Materials and Methods section.

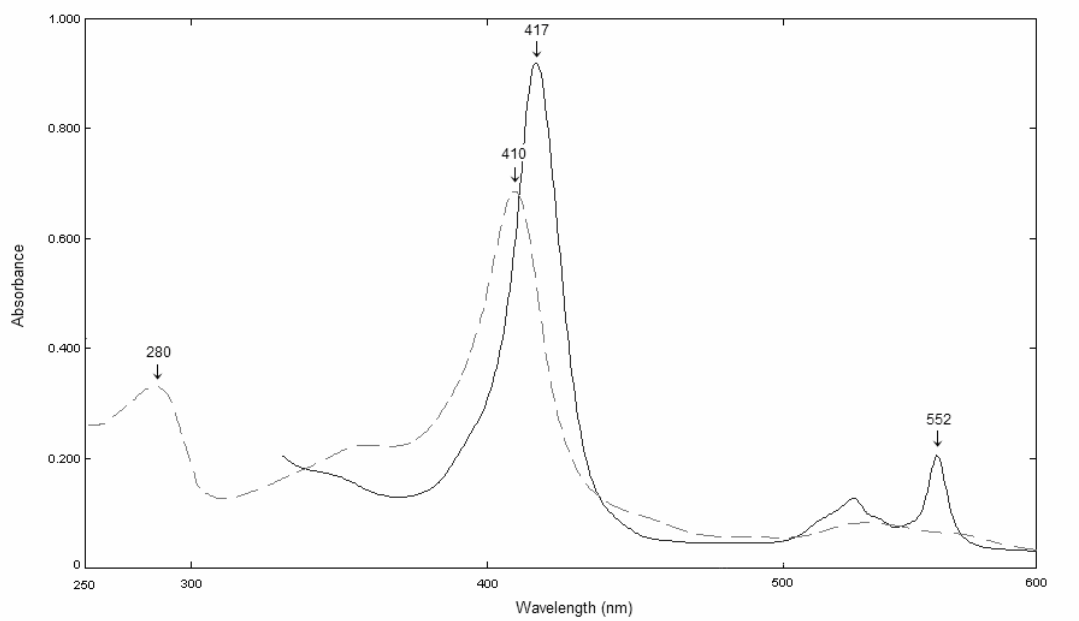

Figure 16: Absorption spectra of (----) ferricyanide - oxidized and (——) ascorbate - reduced cytochrome c_1 head domain. The soret band wavelength for oxidized and reduced cyt c_1 head domain is 410nm and 417 nm, respectively. Its α-band wavelength is 552nm with an extinction coefficient of 17.5 $mM^{-1}.cm^{-1}$. . Protein concentration used is 0.2mg/ml in 20mM Tris-HCl buffer, pH 7.4 containing 20mM NaCl.

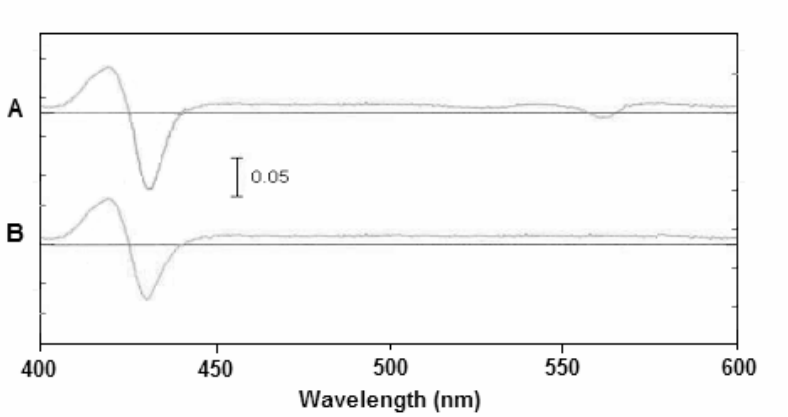

Figure 17: Carbon monoxide optical difference spectra of (A) the wild type cyt bc_1 complex and (B) the cyt c_1 head domain. Carbon monoxide binding was analyzed on the basis of the calculation from specR+CO minus specR spectra as described in Materials and Methods.

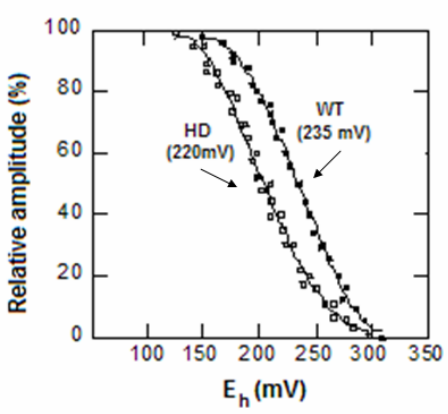

Figure 18: Potentiometric titration of cyt c_1 in purified cytochrome bc_1 complexes from Wild type and from head domain. Plots legend: [▪] Wild type cyt c_1 (WT); Em = 235mV, and [▫] cyt c_1 head domain (HD); Em = 220mV. Oxidative and reductive titrations were performed as described in Materials and Methods. The data were fit to the Nernst equation for n=1.

electron acceptor, cyt c_2, to establish without ambiguity the nature of interaction between the two proteins upon binding, which is necessary for electron transfer.

D. Interaction studies between cytochrome c_1 and cytochrome c_2

Thermotropic properties of each of *Rb. spharoides* cyt c_1 head domain and cyt c_2 were studied using differential scanning calorimetry under different salt concentrations. Both cytochromes exhibit a single endothermodenaturation peak with a varying thermodenaturation temperature based on the redox state of the protein and the salt concentration. The thermodenaturation temperatures, or melting temperatures (Tm), values are listed in Table 4. The Tm for ferri- and ferrocytochrome c_1 head domain is measured to be 55.2 ºC and 56.9 ºC, respectively, at low ionic strength in 20mM Tris Cl, pH 7.4. At the given conditions, the Tm values for ferri- and ferrocytochrome c_2 are measured to be 55.3 ºC and 72.2 ºC, respectively. At high ionic strength, in 20mM TrisCl pH 7.4, 150mM NaCl, the Tm for ferri- and ferrocytochrome c_1 head domain is measured to be 56.6 ºC and 72.2 ºC, respectively. At the given conditions, the Tm values for ferri- and ferrocytochrome c_2 are measured to be 60.2 ºC and 72.8 ºC, respectively. These results indicate that the structural difference between the ferri and ferrocytochrome c_2 is more distinct than that between ferri- and ferrocytochrome c_1 head domain at low ionic strength, while the reverse is true at high ionic strength.

Cyt c2	Low Salt		High Salt	
	Tm	ΔH	Tm	ΔH
Oxidized	55.3 ºC	48	60.2ºC	51
Reduced	72.2 ºC	56	72.8 ºC	56
Cyt c_1 HD	Low Salt		High Salt	
	Tm	ΔH	Tm	ΔH
Oxidized	55.2ºC	27	56.6ºC	28
Reduced	56.9ºC	28	72.2ºC	39

Table 4: Thermotropic properties of cytochrome c_1 head domain (HD) and cytochrome c_2 at different redox state and ionic strength. At low salt concentration, proteins were diluted with 20mM TrisCl, pH 7.4. At high salt concentration, proteins were diluted with 20mM TrisCl, pH 7.4, 150mM NaCl. Tm refers to the melting temperature or the endothermic temperature. ΔH, change in enthalpy, is expressed in Kcal/mol. The data given in this table is the average of two experimental data.

To study the interaction between cyt c_1 head domain and cyt c_2, the two proteins were mixed together at different ionic strength and subjected to DSC. In low ionic strength, the two proteins behave as a complex showing a single endothermodenaturation peak with an endothermic transition temperature of 56.0 ºC (Figure 19). In high ionic strength, each of the cytochromes show a separate endothermodenaturation peak with a Tm of 50.2 ºC for cyt c_1 head domain and 72.0 ºC for cyt c_2. The heat capacity absorbed during the thermodenaturation of the cytochromes is similar to the individual proteins, where cyt c_2 shows a larger enthalpy change than cyt c_1 head domain due to the higher stability of the former. The change in environment seems to affect cyt c_1 head domain stability, shown by a decrease in melting temperature as compared to the individual protein, but not cyt c_2's. The addition of stigmatellin to the cyt c_1 head domain- cyt c_2 mixture, at either low or high ionic concentration, does not affect the thermotropic properties of the proteins and thus the interaction between the two cytochromes. These results clearly show that the two proteins form a complex at low ionic strength, stabilized by electrostatic interaction, which are disrupted upon increasing the ionic strength of the environment.

Additionally, binding between the cyt c_1 head domain and cyt c_2 was measured by gel filtration chromatography on Biogel P-60 at either 20 or 170mM ionic strength, as shown in Figure 20. At low ionic strength, cyt c_1 head domain and cyt c_2 comigrate in solution with and elute as a complex with an apparent molecular weight of 42KDa.

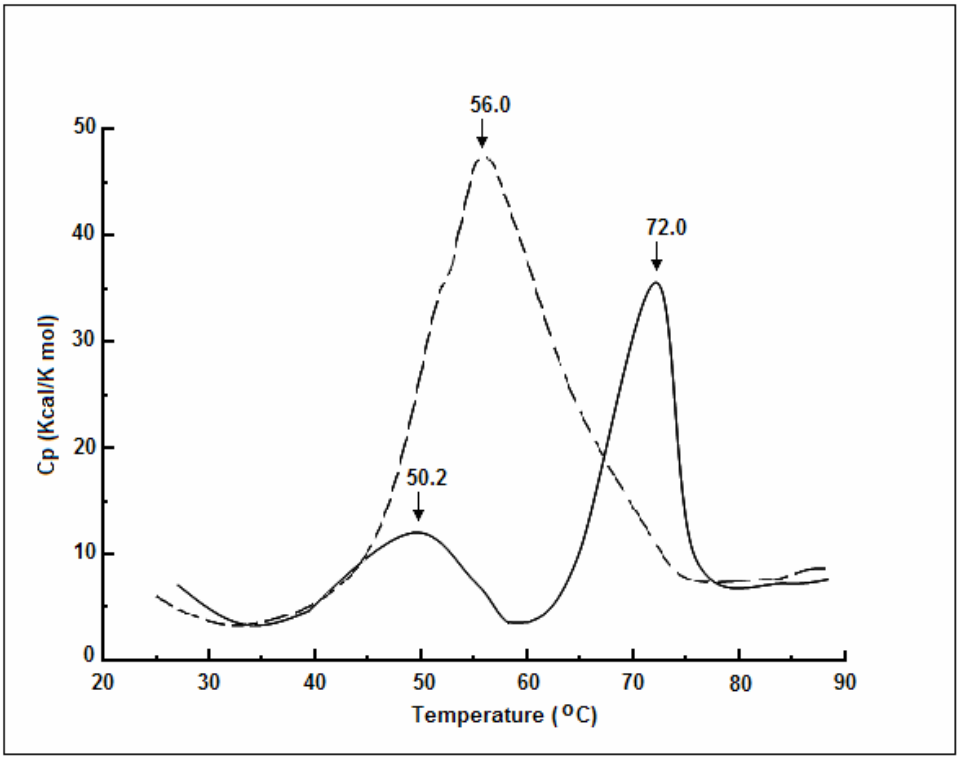

Figure 19: Effect of ionic strength on the complex formation between cytochrome c_1 head domain and cytochrome c_2. Proteins (10nmoles of each) were mixed in (---) 20mM TrisCl, pH 7.4 and (——) 20mM TrisCl, pH 7.4, 150mM NaCl, incubated on ice for 20mns then subjected to DSC as described in Materials and Methods.

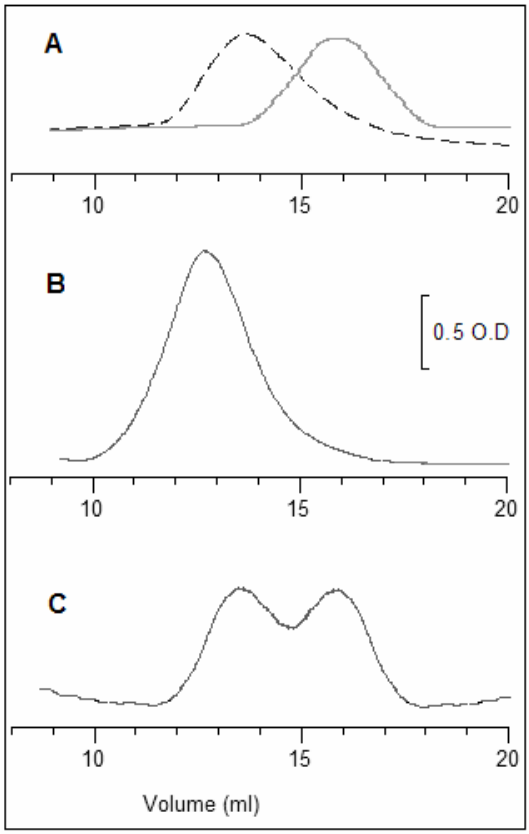

Figure 20: Gel filtration chromatography of complex formation between cyt c_1 head domain and cytochrome c_2 monitored at 280nm. Equimolar amounts of each protein (10 nmoles) were chromatographed (A) separately, showing (---) cyt c_1 head domain and (——) cyt c_2, and together at (B) low and (C) high ionic strength. Samples were passed through a Biogel P-60 column equilibrated with 20mM TrisCl, pH 7.4 in low ionic conditions and 20mM TrisCl, pH 7.4, 150mM NaCl in high ionic conditions as described in Materials and Methods.

However, at high ionic strength, cyt c_1 head domain and cyt c_2 elute separately, at expected positions identical to their single peaks shown in Panel A. These results conclusively demonstrate that the two proteins associate at low ionic strength and form a stable complex, which is disrupted by destabilizing the inter-electrostatic interactions upon increasing the surrounding ionic strength.

To support this hypothesis and study the effect of stigmatellin on the complex formation between cyt c_1 and cyt c_2, thermotropic studies were conducted using wild type cyt bc_1 complex, instead of cyt c_1 head domain, in the presence and absence of stigmatellin at different salt concentrations. As shown in Figure 21, intact cyt bc_1 complex forms a complex with cyt c_2 at low ionic strength showing a single endothermic peak with a melting temperature of 50.0 ºC. The complex can not be formed at high ionic strength, which confirms the hypothesis that high salt concentrations in the vicinity of the complex destabilize the electrostatic interactions between cyt c_1 and cyt c_2 preventing complex formation.

To study the effect of stigmatellin on the surface properties of cyt c_1 and thus on the interaction between cyt c_1 and cyt c_2, the cyt bc_1 complex was treated with stigmatellin before mixture and incubation with cyt c_2. When subjected to DSC, the observed thermotropic properties of the protein mixture reveal no stable complex formation in low ionic strength, as observed with active cyt bc_1 complex (Figure 22).

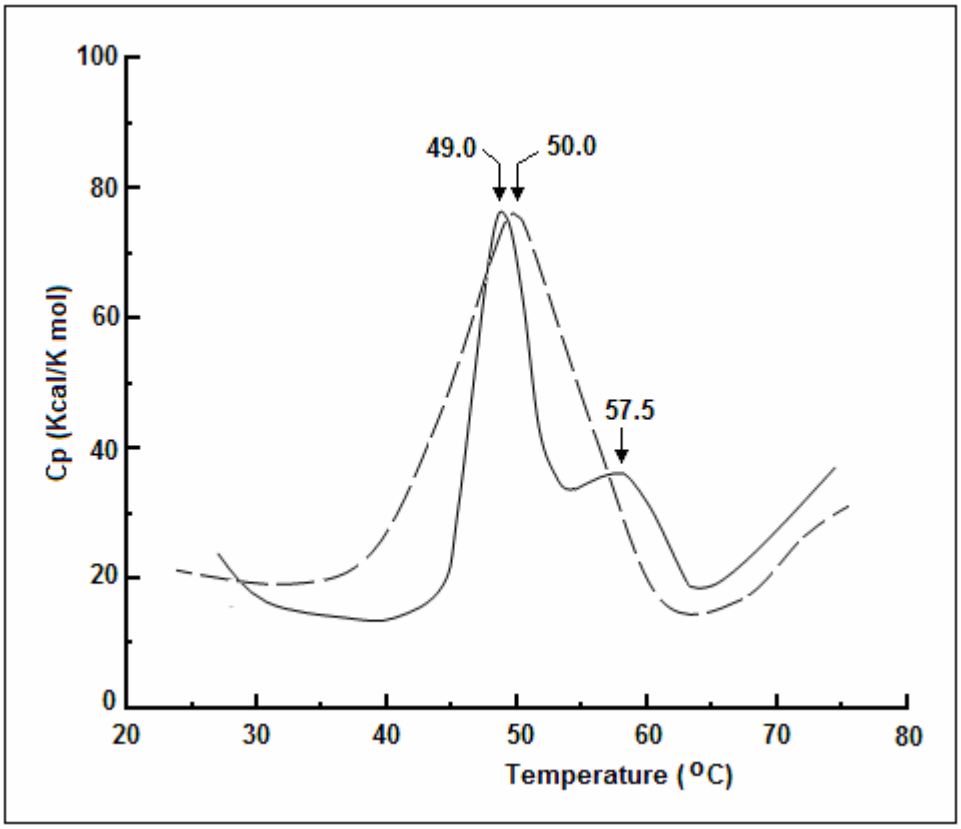

Figure 21: Effect of ionic strength on the complex formation between cytochrome bc_1 complex and cytochrome c_2. Proteins (10nmoles of each) were mixed in (---) 20mM TrisCl, pH 7.4 and (___) 20mM TrisCl, pH 7.4, 150mM NaCl, incubated on ice for 20mns then subjected to DSC as described in Materials and Methods.

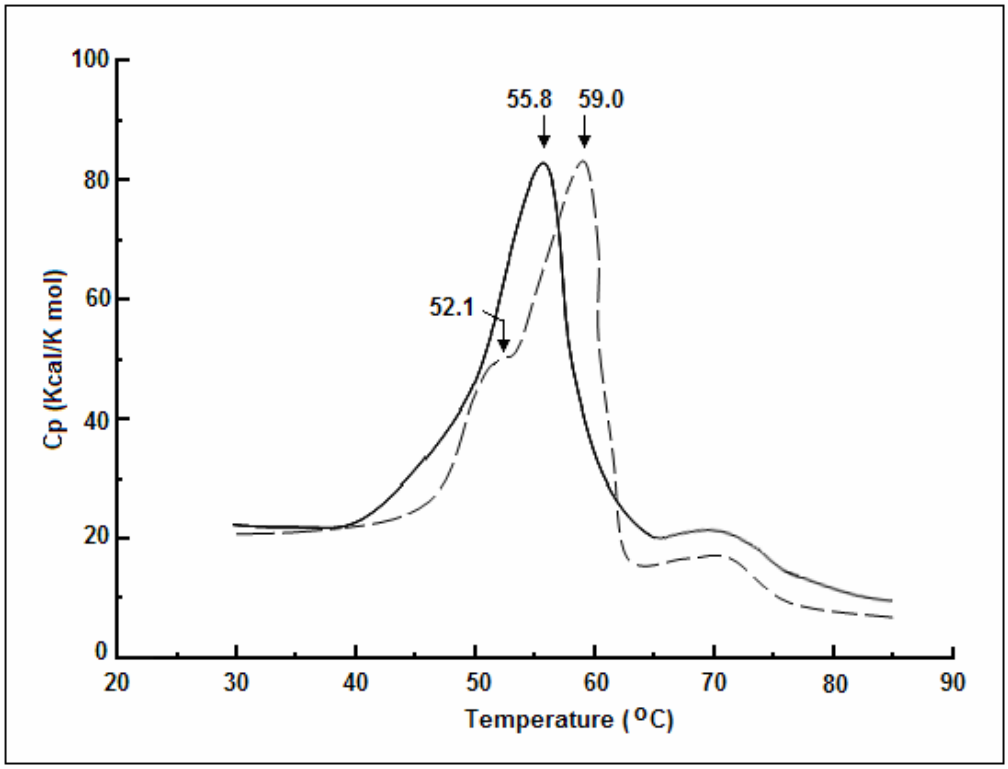

Figure 22: Effect of ionic strength on the complex formation between stigmatellin-bound cytochrome bc_1 complex and cytochrome c_2. The cyt bc_1 complex (10nmoles) in (---) 20mM TrisCl, pH 7.4 and (——) 20mM TrisCl, pH 7.4, 300mM NaCl, was first treated with stigmatellin (30nmoles) and incubated on ice for 20mns followed by the addition of cyt c_2 (10nmoles) and incubation on ice for 15mns before being subjected to DSC as described in Materials and Methods. At low salt concentration, the stigmatellin-bound cyt bc_1 complex and cyt c_2 show two peaks with Tm values of 53.1 ºC and 59 ºC, respectively. At high salt concentration, the two proteins form a complex with a Tm value of 55.8 ºC.

Instead, two peaks are detected with melting temperatures of 52.1 ºC and 59.0 ºC, corresponding to cyt bc_1 complex and cyt c_2, respectively. Although no stable complex is formed at such conditions, an interaction between the two proteins still exists depicted by the overlap of the two endothermic peaks. However, a single endothermodenturation peak is observed at high ionic strength, in 20mM TrisCl, pH 7.4, 300mM NaCl, with a Tm of 55.8 ºC, implying complex formation between stigmatellin-bound cyt bc_1 complex and cyt c_2 at such conditions (Figure 22). These results suggest that upon stigmatellin binding to the cytochrome bc_1 complex, the surface of cyt c_1 head domain undergoes structural modifications exposing a more hydrophobic face and favoring hydrophobic interactions with cyt c_2, which are stabilized at high ionic strength. Since stigmatellin is known to bind the cyt *b* subunit at the Qo site, its effect on cyt c_1 must be indirect, possibly through the cyt *b* subunit itself. At this point, the mechanism for cyt c_1 head domain structural modification remains unknown but further studies, using the cyt c_1 head domain, can help better understand the specifics behind such modifications.

To further clarify the change in Tm values under different conditions, wild type cyt bc_1 complex was subjected to DSC in the presence and absence of stigmatellin at low and high ionic strength. In the absence of stigmatellin, active cyt bc_1 complex show a single endothermic peak with Tm values of 45.0 ºC and 46.0 ºC, at low and high ionic strength, respectively (Figures 23A). When treated with stigmatellin, the cyt bc_1 complex

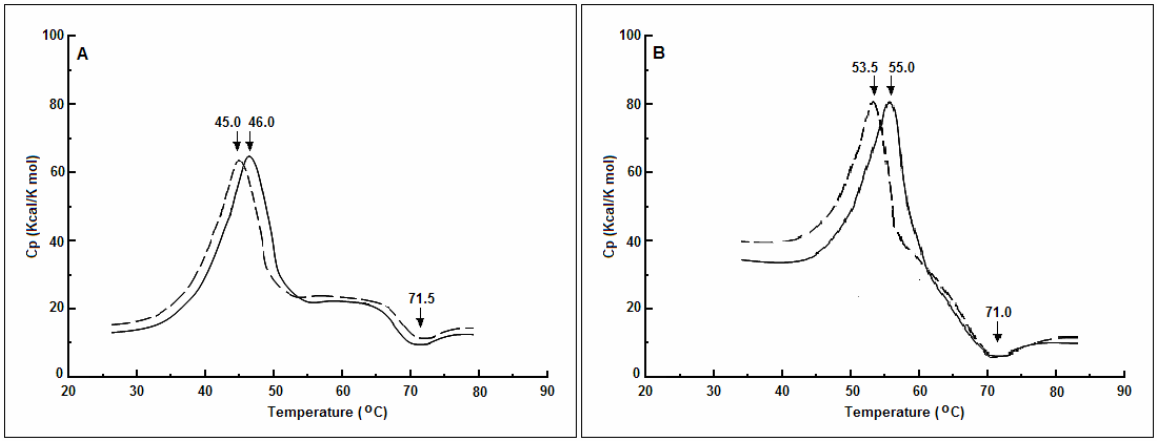

Figure 23: Differential scanning calorimetry thermograms of wild type cyt bc_1 complex. (A) The cyt bc_1 complex (10nmoles) thermotropic properties at (---) low ionic strength, in 20mM TrisCl, pH 7.4, 0.3% β - OG, with Tm = 45.0 ºC and (——) high ionic strength, in 20mM TrisCl, pH 7.4, 0.3% β-OG, 150mM NaCl, with Tm = 46 ºC and (B) stigmatellin-bound cyt bc_1complex (10nmoles) thermotropic properties at (---) low ionic strength, in 20mM TrisCl, pH 7.4, 0.3% β – OG, with Tm = 53.5 ºC and (——) high ionic strength, in 20mM TrisCl, pH 7.4, 0.3% β-OG, 150mM NaCl, with Tm = 55.0 ºC, were recorded using DSC, as described in Materials and Methods.

exhibits an endothermic peak with Tm values of 53.5 ºC and 55.0 ºC, at low and high ionic strength, respectively, followed by an exothermic peak with an exothermal temperature of 71.0 ºC (Figures 23B).

These results show that the association of cyt c_2 with the cyt bc_1 complex through electrostatic interactions, at low ionic strength in the absence of stigmatellin, stabilizes the cyt bc_1 complex with a Tm increase of 5.0 ºC. At high ionic strength, the association of cytochrome c_2 with stigmatellin bound cyt bc_1 complex does not affect the stability of the protein as no significant change in the thermodenaturation temperature is observed.

The exothermic peak observed in the wild type data is present in all conditions, in the presence or absence of stigmatellin and at high or low ionic strength. Therefore, it is believed to be a property of the cytochrome bc_1 complex, which is most likely due to exothermic aggregation of the protein at high temperatures.

E. Conclusion

The soluble cyt c_1 head domain is stable and retains the same properties as the membrane-bound wild type cyt c_1 and interacts in vitro with its natural oxidant, cytochrome c_2. Study of changes in thermotropic properties, using DSC, upon the interaction between the two proteins during complex formation has provided important information about the nature of the interaction under different conditions. Results imply

that at pH 7.4, the cyt bc_1-cyt c_2 complex is predominantly maintained by electrostatic interactions, which are disrupted by high ionic strength. Upon binding of stigmatellin to the cyt bc_1 complex, the cyt c_1 interface seems to undergo structural changes resulting in exposure of a hydrophobic patch, favoring non-polar interactions with cyt c_2, which are rather stabilized by high ionic strength. The mechanism of cyt c_1 head domain structural change remains unknown at this time, as further experiments need to be conducted to depict the effect of binding of stigmatellin, which binds at the Qo pocket of the cyt *b* subunit, on the soluble domain of cyt c_1.

This study clarifies the ambiguous questions of the nature of the interaction between the cytochrome bc_1 complex and its electron acceptor, cytochrome c_2. Additionally, it provides an elaborate method to isolate and purify an intact and fully active cytochrome c_1 head domain, which can be useful in further functional and structural characterization through mutagenic studies to specifically identify the amino acids, on the surface of cytochrome c_1, involved in the formation of the cyt c_1- cyt c_2 complex when either hydrophilic or hydrophobic interaction is involved.

REFERENCES

1. Hauska, G., Hurt, E., Gabellini, N., and Lockau, W. (1983) *Biochim. Biophys. Acta* **726**, 97-133

2. Hatefi, Y. (1985) *Annu Rev Biochem* **54**, 1015-1069

3. Trumpower, B. L. (1990) *Microbiol. Rev.* **54**, 101-129

4. Trumpower, B.L., and Gennis R. B. (1994) *Annu. Rev. Biochem.* **63**, 675-716

5. Berry, E. A., Guergova-Kuras, M., Huang, L. S., and Crofts, A. R. (2000) *Annual Rev. Biochem.* **69**, 1005-1075

6. Schagger, H., Brandt, U., Gencic, S., and Von Jagow, G. (1995) *Methods Enzymol.* **260**, 82-96

7. Ljungdahl, P. O., Pennoyer, J. D., Robertson, D. E., and Trumpower, B. L. (1987) *Biochim. Biophys. Acta* **891**, 227-241

8. Yu, L., Tso, S. C., Shenoy, S.K., Quinn, B. N., and Xia, D. (1999) *J. Bioenerg. Biomembr.* **31**, 251-257

9. Robertson, D. E., Ding, H., Chelminski, P. R., Slaughter, C., Hsu, J., Moomaw, C., Tokito, M., Daldal, F., and Dutton, P. L. (1993) *Biochemistry* **32**, 1310-1317

10. Yu, L., Tso, S. C., Shenoy, S. K., Quinn, B. N., and Xia, D. (1999) *J. Bioenerg. Biomembr.* **3**, 251-257. Review

11. Mitchell, P. (1976) *J Theor Biol* **62**, 327-367

12. Crofts, A. R., Shinkarev, V. P., Kolling, D. R., and Hong, S. (2003) *J Biol Chem*. **278**, 36191-36201

13. Trumpower, B. L. (1990) *J Biol Chem* **265**, 11409-11412

14. Gao, X., Wen, X., Yu, C., Esser, L., Tso, S., Quinn, B., Zhang, L., Yu, L., and Xia, D. (2002) *Biochemistry* **41**, 11692-11702

15. Zhang, Z., Huang, L., Shulmeister, V. M., Chi, Y. I., Kim, K. K., Hung, L. W., Crofts, A. R., Berry, E. A., and Kim, S. H. (1998) *Natur*e **392**, 677-684

16. Hunte, C., Koepke, J., Lange, C., Rossmanith, T., and Michel, H. (2000) *Structure Fold Des* **8**, 669-684

17. Yu, C. A., Xia, J. Z., Kachurin, A. M., Yu, L., Xia, D., Kim, H., and Deisenhofer, J. (1996) *Biochim Biophys Acta* **1275**,47-53. Review

18. Xiao, K., Chandrasekaran, A., Yu, L., and Yu, C. A. (2001) *J Biol Chem* **276**, 46125-46131

19. Gong, X., Yu, L., Xia, D., and Yu, C. A. (2005) *J. Biol. Chem*. **280**, 9251-9257

20. Kim, H., Xia, D., Yu, C.A., Xia, J. Z., Kachurin, A. M., Zhang, L., Yu, L., ND Deisenhofer, J. (1998) *Proc Natl Acad Sci USA* **95**, 8026-8033

21. Gao, X., Wen, X., Esser, L., Quinn, B., Yu, L., Yu, CA., and Xia, D. (2003) *Biochemistry* **42**, 9067-80

22. Esser, L., Quinn, B., Li, Y.F., Zhang, M., Elberry, M., Yu, L., Yu, C.A., and Xia, D. (2004) *J Mol Biol*. **341**, 281-302.

23. Tian, H., Yu, L., Mather, M. W., and Yu, C. A. (1998) *J. Biol. Chem*. **273**, 27953-27959

24. Tian, H., White, S., Yu, L., and Yu, C.A. (1999) *J. Biol. Chem*. 274, 7146-7152

25. Xiao, K., Yu, L., and Yu, C. A. (2000) *J. Biol. Chem*. **275**, 38597-38604

26. Yu CA, Tian H, Zhang L, Deng KP, Shenoy SK, Yu L, Xia D, Kim H, and Deisenhofer J. (1999) *J. Bioenerg Biomembr.* **3**,191-199. Review

27. Trumpower, B. L., and Haggerty, J. G. (1980) *J. Bioenerget. Biomembr.* **12,** 151-164

28. Von Jagow, G., Gribble, G. W., and Trumpower, B. L. (1986) *Biochemistry* **25,** 775-780

29. Sauter, H., Steglich, W., and Anke, T. (1999) *Angew. Chem. Int. Ed.* **38,** 1328-1349

30. Jordan, D. B., Livingston, R. S., Bisaha, J. J., Duncan, K. E., Pember, S. O., Picollelli, M. A., Schwartz, R. S., Sternberg, J. A., and Tang, X. S. (1999) *Pesticide Science* **55,** 105-118

31. Kessl, J. J., Lange, B. B., Merbitz-Zahradnik, T., Zwicker, K., Hill, P., Meunier, B., Palsdottir, H., Hunte, C., Meshnick, S., and Trumpower, B. L. (2003) *J. Biol. Chem.* **278,** 31312-31318

32. DiMauro, S., and Schon, E. A. (2003) *N. Engl. J. Med.* **348,** 2656-2668

33. Andreu, A. L., Hanna, M. G., Reichmann, H., Bruno, C., Penn, A. S., Tanji, K., Pallotti, F., Iwata, S., Bonilla, E., Lach, B., Morgan-Hughes, J., and Di-Mauro, S. (1999) *N. Engl. J. Med.* **341,** 1037-1044

34. Brown, M. D., Voljavec, A. S., Lott, M. T., Torroni, A., Yang, C. C., and Wallace, D. C. (1992) *Genetics* **130,** 163-173

35. Turrens, J. F., Alexandre, A., and Lehninger, A. L. (1985) *Arch. Biochem. Biophys.* **237,** 408-414

36. Staniek, K., Gille, L., Kozlov, A. V., and Nohl, H. (2002) *Free Radical Res.* **36,** 381-387

37. Yu, C. A., and Yu, L. (1982) *Biochemistry* **21**, 4096-4101

38. Mather, M. W., Yu, L., and Yu, C. A. (1995) *J. Biol. Chem*. **270**, 28668-28675

39. Tian, H., Yu, L., Mather, M. W., and Yu, C. A. (1997) *J. Biol. Chem*. **272**, 23722-23728

40. Berden, J. A., and Slater, E. C. (1970) *Biochim. Biophys. Acta* **216**, 237-249

41. Yu, L., Dong, J. H., and Yu, C. A. (1986) *Biochim. Biophys. Acta* **852**, 203-211

42. Bartsch, R. (1978) Plenum Press New York, 249-279

43. Laemmli, U. K. (1970). *Nature* **227**, 680-685

44. Dutton, P. L. (1978) *Methods Enzymol*. **54**, 411-435

45. Guner, S., Robertson, D. E., Yu, L., Qiu, Z. H., Yu, C. A., and Knaff, D. B. (1991) *Biochim. Biophys. Acta* **1058**, 269-279

46. Z. Otwinowski, W. Minor, *Meth. Enzym.* **276** (1997) 307-326

47. Xia, D., Yu, C. A., Kim, H., Xia, J. Z., Kachurin, A. M., Zhang, L., Yu, L., and Deisenhofer, J. (1997) *Science* **277,** 60-66

48. Zhang, Z., Huang, L., Shulmeister, V. M., Chi, Y. I., Kim, K. K., Hung, L. W., Crofts, A. R., Berry, E. A., and Kim, S. H. (1998) *Nature* **392,** 677-684

49. Iwata, S., Lee, J. W., Okada, K., Lee, J. K., Iwata, M., Rasmussen, B., Link, T. A., Ramaswamy, S., and Jap, B. K. (1998) *Science* **281,** 64-71

50. Hunte, C., Koepke, J., Lange, C., Rossmanith, T., and Michel, H. (2000) *Structure* **15,** 669-684

51. Kurisu, G., Zhang, H., Smith, J. L., and Cramer, W. A. (2003) *Science* **302,** 1009-1014

52. Stroebel, D., Choquet, Y., Popot, J. L., and Picot, D. (2003) *Nature* **426,** 413-418

53. Kim, H., Xia, D., Yu, C. A., Xia, J. Z., Kachurin, A. M., Zhang, L., Yu, L., and Deisenhofer, J. (1998) *Proc. Natl. Acad. Sci. U. S. A.* **95,** 8026-8033

54. Lange, C., Nett, J. H., Trumpower, B. L., and Hunte, C. (2001) *EMBO J.* **20,** 6591-6600

55. Gao, X., Wen, X., Yu, C., Esser, L., Tsao, S., Quinn, B., Zhang, L., Yu, L., and Xia, D. (2002) *Biochemistry* **41,** 11692-11702

56. Lange, C., and Hunte, C. (2002) *Proc. Natl. Acad. Sci. U. S. A.* **99,** 1800-2805

57. Gao, X., Wen, X., Esser, L., Yu, L., Yu, C. A., and Xia, D. (2003) *Biochemistry* **42,** 9067-9080

58. Hunte, C., Palsdottir, H., and Trumpower, B. L. (2003) *FEBS Lett.* **545,** 39-46

59. Esser, L., Quinn, B., Li, Y., Zhang, M., Elberry, M., Yu, L., Yu, C. A., and Xia, D. (2004) *J. Mol. Biol.* **341,** 281-302

60. Huang, L., Cobessi, D., Tung, E. Y., and Berry, E. A. (2005) *J. Mol. Biol.* **35,** 573-597

61. Berry, E. A., Huang, L., Saechao, L. K., Pon, N. G., Valkova-Valchanova, M., and Daldal, F. (2004) *Photosynthesis Res.* **81,** 251-275

62. Liu, X., Yu, C. A., and Yu, L. (2004) *J. Biol. Chem.* **279,** 47363-47371

63. Esser, L., Gong, X., Yang, S., Yu, L., Yu, C. A., and Xia, D. (2006) *Proc. Natl. Acad. Sci. U. S. A.* **103,** 13045-13050

64. Elberry, M., Yu, L., and Yu, C. A. (2006) *Biochemistry* **45,** 4991-4997

65. Xiao, K., Liu, X., Yu, C. A., and Yu, L. (2004) *Biochemistry* **43,** 1488-1495

66. Chen, Y. R., Yu, C. A., and Yu, L. (1996) *J. Biol. Chem.* **271,** 2057-2062

67. Rodgers, S., Moser, C., Martinez-Julvez, M., and Sinning, I. (2000) *Eur. J. Biochem.* **267,** 3753-3761

68. Yu, L., Tso, S. C., Shenoy, S. K., Quinn, B. N., and Xia, D. (1999) *J. Bioenerget. Biomembr.* **31,** 251-257

69. Stonehuerner, J., Williams, J. B., and Millett, F. (1979) *Biochemistry* **18**, 5422-5428

70. Margoliash, E., and Bosshard, H.R. (1983) *Trends Biochem. Sci*. **8**, 316-320

71. Hall, J., Zha, X., Yu, L., Yu, C.A., and Millett, F. (1989) *Biochemistry* **28**, 2568-2571

72. Guner, S., Willie, A., Millett, F., Caffrey, M., Cusanovich, M., Robertson, D., and Knaff, D. (1993) *Biochemistry* **32**, 4793-4800

73. Hall, J., Zha, X., Yu, L., Yu, C.A., and Millett, F. (1987) *Biochemistry* **26**, 4501-4504

74. Stonehuerner, J., O'Brien, P., Geren, L., Millett, F., Steidl, J., Yu, L., Yu., C.A. (1985) *J. Biol. Chem*. **260**, 5392-5398

75. Heacock, D., Liu, R. Q., Yu, C.A., Yu, L., Durham, B., and Millett F. (1993) *J. Biol. Chem* **268**, 27171-27175

76. Lange, C., and Hunte, C. (2001) *PNAS*. **99**, 2800-2805

77. Hunte, C., Solmaz, S., and Lange, C. (2002) *Biochim. Biophys. Acta* **1555**, 21-28

78. Engstrom, G., Rajagukguk, R., Saunders, A. J., Patel, C. N., Rajagukguk, S., Merbitz-Zhradnik, T., Xiao, K., Pielak, G. J., Trumpower, B., Yu, C.A., Yu, L., Durham, B. and Millett, F. (2003) *Biochem*. **42**, 2816-2824.

79. Yu, L., Dong, J.H., and Yu, C.A. (1986) *Biochim. Biophys. Acta* **852,** 203-211

80. Konishi, K., Van Doren, S., Kramer, D., Crofts, A., and Gennis, R. (1991) *J. Biol. Chem*. **266**, 14270-14276

VITA

Maria Elberry

Candidate for the Degree of

Doctor of Philosophy

Thesis: STUDIES OF THE CYTOCHROME bc_1 COMPLEX FROM *RHODOBACTER SPHAEROIDES*

Major Field: Biochemistry and Molecular Biology

Biographical:

Personal Data: Born in Ghosta, Lebanon, on October 29, 1981. Proud Daughter of Antoine Elberry and Joumana Saber.

Education: Graduated from Saint Coeurs-Kfarahbab High school in June 1999; Received Bachelor Degree in Biology from Lebanese American University, Byblos, Lebanon, in June 2002. Received Masters of Science degree in Biochemistry and Molecular Biology from Oklahoma State University, Stillwater, Oklahoma in December 2005. Completed requirements for the Doctor of Philosophy degree at Oklahoma State University in July 2008.

Name: Maria Elberry Date of Degree: July 2008
Institution: Oklahoma State University Location: Stillwater

Title of Study: STRUCTURAL STUDIES OF THE CYTOCHROME bc_1 COMPLEX FROM *RHODOBACTER SPHAEROIDES*

Pages in Study: 80 Candidate for the Degree of Doctor of Philosophy

Major Field: Biochemistry and Molecular Biology

Scope and Method of Study: Determine the structure of *Rhodobacter sphaeroides* cytochrome bc_1 complex using the engineered Super Reductase double mutant and studying the interaction between cytochrome c_1 head domain and its electron acceptor, cytochrome c_2. Studies were done using a variety of genetic and biochemical techniques.

Findings and Conclusions: The critical importance of cytochrome bc_1 complex has made it a target for numerous antibiotics, fungicides, and anti-parasitic agents. The elucidation of the molecular mechanisms underlying these phenomena requires a combination of experimental approaches and in particular, structural investigations that can provide a molecular framework for further experiments. Because of the importance of the bacterial cyt bc_1 complex in functional studies, a high resolution structure has been actively pursued for many years. In this study, we report an engineered mutant of *Rb. sphaoeroides* cyt bc_1 complex, the SR mutant-SuperReductase that conspicuously shows higher enzymatic activity and significant increase in protein stability as compared to the wild type. The discovery of such an active and stable protein provided a breakthrough in the structure determination of *Rb. sphaeroides* cyt bc_1 complex, providing a vital understanding of the structural-functional relationship of the complex. Additionally, cyt c_1 head domain, the site of interaction between the cyt bc_1 complex and its electron acceptor cytochrome c_2, is isolated and purified to study without ambiguity the nature of interaction between the two proteins using differential scanning calorimetry.

ADVISER'S APPROVAL: _____

Dr. Chang-An Yu